Supporting Information for:

Variable Temperature Kinetic Isotope Effects Demonstrate Extensive Tunnelling in the C–H Activation of a Transition Metal-Oxo Complex

Joseph E. Schneider, McKenna K. Goetz, and John S. Anderson

Department of Chemistry, The University of Chicago, Chicago, IL 60637, United States

Correspondence to: jsanderson@uchicago.edu

Contents

Experimental Methods and Data

Unless stated otherwise, all manipulations were performed under an inert atmosphere in MBraun gloveboxes or using standard Schlenk techniques. PhB(^{t}BuIm)$_3$Co^{III}O (**CoO**), d_1-fluorene, d_2-fluorene, and d_4-DHA were synthesized according to literature procedures;[1–4] all other chemicals were obtained from commercial sources. We found that to selectively obtain d_1-fluorene and not d_2-fluorene it was critical to use exactly one equivalent of n-butyllithium and to rapidly quench with D_2O. For d_2-fluorene and d_4-DHA, we found using enough d_6-DMSO to fully dissolve the starting substrate allowed us to achieve higher isotopic purity but suspect heating the reaction only resulted in decreased yield. All substrates were recrystallized from hot hexanes prior to use.

Measurement of KIEs by Competition Experiments

Competition experiments were run with 1.25 mM of **CoO** and 20 equivalents of substrate in 2.0 mL of toluene. In a typical experiment, the substrate was dissolved in 1.9 mL of solvent and equilibrated to the desired temperature (a sealed vial in the glovebox freezer for 239 K data, a Unisoku USP-203-B cryostat for 263 K data, a taped vial in an out of glovebox ice bath for 273 K data, a sealed vial set on the glovebox floor for 296 K data, and a sealed vial set in a glovebox heat block for 323 K data), then 100 μL of **CoO** stock solution (25 mM) was added via syringe. The reaction was run to > 99% completion, as determined by five time constants (inverse rate constant) of the expected rate for the 10 equivalents of reactive C–H bonds based on an Arrhenius analysis of the fluorene d_0-kinetic data (see below). After the reaction, it was passed through either alumina or silica to remove Co containing products, dried, redissolved in DCM, and analyzed by GC-MS. See below for yield measurements and a discussion of their significance.

GC-MS analysis was performed with an Agilent 7890B GC system and Agilent 4977A MSD. Chemical ionization was used to avoid fractionation. The amount of each isotopomer was determined by measuring a reference spectrum with no deuterium and fitting the partially deuterated spectra to a sum of the reference spectra shifted by each possible amount of deuterium; i.e. intensity at m/z was modeled as $inten_m = \sum ref_{m-n} p_n$; with ref_{m-n} being the intensity of the reference spectra at m/z-n and p_n giving the amount of d_n-compound in the mixture; these p_n were fit with least squares and then normalized to add to 1. A weighted sum of the amount of deuterium in each isotopomer could be used for a total amount proportion of deuterium p_D in each sample ($p_D = \sum p_n n$). Fluorene was fit for m/z = 195–199, DHA was fit to m/z = 209–215, and bifluoreneyl fit to m/z = 331–335. The Fluorene and DHA peaks correspond to ionization with $C_2H_5^+$, which were used to avoid complications with hydride/deuteride loss which complicated the features for ionization with H^+. No M–1 peak was observed for bifluorenyl, so the more intense peak with H^+ ionization was used. The experimental data was modeled with the formula:

$$\frac{p_{PH}}{p_{PD}} = \frac{2k_{SH_2}p_{SH_2} + k_{SDH}p_{SHD}}{k_{SHD}p_{SD_2} + 2k_{SD_2}p_{SHD}} = \frac{2KIE^{1^\circ}KIE^{2^\circ}p_{SH_2} + KIE^{2^\circ}p_{SHD}}{KIE^{1^\circ}p_{SHD} + 2p_{SD_2}} \quad \textbf{(S1)}$$

where the p_P values indicate the proportions of protons/deuterons in the product, the p_S values indicate the proportion of the indicated isotopomer in the substrate, and the kS values indicate the rate of reaction with the indicated isotopomer (k_{SHD} refers to abstraction of an H–atom with a

secondary D–atom, and vice-versa for k_{SDH}). See Scheme S1 for an illustration of equation (S1) in the ideal case of pure d_1-fluorene and 1:1 d_0-fluorene:d_2-fluorene.

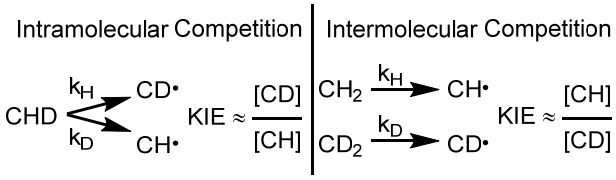

Scheme S1 An illustration of how KIEs are determined by product isotope distribution in competition experiments.

The KIEs were in turn modeled as

$$KIE = \frac{A_H}{A_D} e_a^{\frac{E_a(D)-E_a(H)}{RT}} \quad \textbf{(S2)}$$

with the primary and secondary KIE having separate differences in activation energy $E_a(D) - E_a(A)$ and prefactor ratios A_H/A_D. Individual KIE values at a given temperature were determined by a nonlinear least squares fit of equation (S1) with p_p values from both intramolecular and intermolecular competition. Substituting equation (S2) into equation (S1) and performing a nonlinear least squares fit to all competition data yielded the reported values and errors of $E_a(D) - E_a(A)$ and A_H/A_D. We used mean values of the p_S from three measurements to prevent complicated correlations in error from biasing our best fit parameters; however, if we use any individual measurement of p_S the results do not change within error. We see no evidence for scrambling between product radicals and the substrate in the GCMS peak of unreacted substrate and reported rate constants of C–H scrambling are much smaller than reported dimerization rate constants (see below).

Measurement of KIEs by Kinetic Experiments

UV-vis data were collected with a Thermo Fisher EVO300 LS spectrometer and a Unisoku USP-203-B cryostat. All experiments were run with 1.25 mM of **CoO** with 10 equivalents of substrate in 2 mL of toluene. In a typical experiment, a cuvette was prepared in an N_2 glovebox with 1.8 mL toluene and 100 µL of a stock solution of 250 mM substrate, and then sealed with a screwtop cap with a puncturable septum. The cuvette was allowed to equilibrate to the desired temperature and then 100 µL of 25 mM **CoO** was injected via syringe. The absorbance at 470 nm was followed to ~85% completion, and the rate constant k_{obs} was obtained via a nonlinear least squares fit of the absorbance at 470 nm to $A(t) = A_\Delta e^{-k_{obs}t} + A_\infty$.

For undeuterated substrates, k_H was estimated as the mean of three k_{obs} measurements; the reported error is the standard error of the mean. Three k_{obs} for deuterated substrate were similarly averaged to obtain $k_{D,obs}$ and these were corrected with equation S3 for the actual extent of deuteration in the sample (p_D) to obtain $k_{D,corr}$ values, which is what k_D refers to unless otherwise stated.

$$k_{D,corr} = \frac{1}{p_D}\left(k_{D,obs} - k_H(1 - p_D)\right) \quad \textbf{(S3)}$$

The p_D were determined both by ^{1}H NMR spectroscopy and GC-MS analysis, which closely agreed: For d_2-fluorene, ^{1}H NMR spectrum analysis gave 98% and GC-MS gave 96%; 97% was used. For d_4-DHA, ^{1}H-NMR spectrum analysis gave >99% and GC-MS gave 95-97% (depending on how much of the M+29 peak is assigned to a d_2-anthracene impurity); 98% was used. Error in the estimate of p_D was not propagated because it would lead to complicated correlations between temperature data points which would confound later analysis (assuming this error is in the measurement and not in the sampling of the substrate). Instead, we confirmed that our conclusions are consistent within the whole range of possible p_D values indicated above (Table S4).

KIEs were then calculated as the ratio of k_H and $k_{D,corr}$, with error propagated from k_H and $k_{D,obs}$. Arrhenius parameters $E_a(D)$-$E_a(H)$ and $\ln(A_H/A_D)$ were calculated by a least squares linear fit of ln(KIE) estimates to 1/RT. We also performed a nonlinear least squares fit of values of $E_a(D) - E_a(H)$ and $\ln(A_H/A_D)$ to the experimental k_H and $k_{D,obs}$ and found identical mean estimates and similar error bars.

For d_4-DHA at 263 K, the rate was too slow to follow to completion; instead, we measured initial rates to ~9% completion, with the average A_Δ of other temperatures used to convert the rate from of absorbance per second to a rate constant in per second ($k_{D,obs} = k_{Init}/A_\Delta$, with k_{Init} the slope of the absorbance at 470 nm with time). For error propagation, the standard error of A_Δ was used (not the standard error of the mean). This data point is graphed to demonstrate consistency with the other data points, but not included in the linear fits to variable temperature.

Summary of KIE Estimates at Different Temperatures

A summary of the competition KIE data is given in Table S1. Table S2 and Table S3 give a summary of the kinetic KIE data. Table S4 shows how the assumption of a p_D value affects the resulting VT-KIE parameters from kinetic data. Figure S10-Figure S27 show GC-MS data pertaining to individual competition experiments, and Figure S28-Figure S31 show the exponential fits to kinetic traces.

Table S1. Summary of competition KIE data for the reaction of **CoO** with d_n-fluorene.

Temperature (K)	Intramolecular % H in Product (p_{PH})[a]	Intermolecular % H in Product (p_{PH})[b]	Primary KIE	Secondary KIE
323	27.4(9)%	78.6(7)%	3.6(1)	1.18(4)
296	27.3(6)%	78.2(2)%	3.57(8)	1.16(2)
273	25.9(9)%	79.6(3)%	3.9(1)	1.17(3)
263	25.2(7)%	80.2(2)	4.1(1)	1.17(2)
239	26(1)%	80.0(5)%	4.0(2)	1.18(4)

Reactions were run with 20 equivalents of fluorene (10 equivalents each of C–H and C–D) and 1.25 mM of cobalt. All proportions were measured in triplicate. Reported errors are the standard errors of the mean. [a]Percentage of benzylic protons in the bifluorenyl product from oxidation of d_1-fluorene. [b]Percentage of benzylic protons in the bifluorenyl product from oxidation of 1:1 d_0-fluorene:d_2-fluorene.

Table S2. Kinetic data for the reaction of **CoO** with fluorene.

Temperature (K)	k_H (1/s)	$k_{D,obs}$ (1/s)	$k_{D,corr}$ (1/s)	KIE[s]	ln(KIE)
323	$2.72(2) \cdot 10^{-2}$	$7.7(3) \cdot 10^{-3}$	$7.1(3) \cdot 10^{-3}$	3.8(2)	1.34(5)
303	$7.47(5) \cdot 10^{-3}$	$2.10(3) \cdot 10^{-3}$	$1.94(3) \cdot 10^{-3}$	3.86(6)	1.35(2)
283	$1.78(2) \cdot 10^{-3}$	$4.60(7) \cdot 10^{-4}$	$4.19(7) \cdot 10^{-4}$	4.24(9)	1.44(2)
263	$3.44(6) \cdot 10^{-4}$	$7.3(2) \cdot 10^{-5}$	$6.5(3) \cdot 10^{-5}$	5.3(2)	1.67(4)

Rates are pseudo-first order rate constants measured with 10 equivalents of fluorene and 1.25 mM of cobalt. All pseudo-first order rate constants (k_H and $k_{D,obs}$) were measured in triplicate. Reported errors are the standard errors of the mean. [a]See below for a discussion of why we believe these are less accurate than the KIEs from competition experiments.

Table S3. Kinetic data for the reaction of **CoO** with DHA.

Temperature (K)	k_H (1/s)	$k_{D,obs}$ (1/s)	$k_{D,corr}$ (1/s)	KIE	ln(KIE)
323	$1.19(1) \cdot 10^{-2}$	$1.26(3) \cdot 10^{-3}$	$1.04(3) \cdot 10^{-3}$	11.4(3)	2.44(3)
303	$3.34(8) \cdot 10^{-3}$	$2.7(1) \cdot 10^{-4}$	$2.1(1) \cdot 10^{-4}$	16(1)	2.76(7)
283	$7.9(1) \cdot 10^{-4}$	$4.6(2) \cdot 10^{-5}$	$3.1(2) \cdot 10^{-5}$	26(1)	3.25(6)
263	$1.49(3) \cdot 10^{-4}$	$6.0(8) \cdot 10^{-6}$ [b]	$3.0(8) \cdot 10^{-6}$	50(10)	3.9(3)

Rates are pseudo-first order rate constants measured with 10 equivalents of DHA and 1.25 mM of cobalt. All pseudo-first order rate constants (k_H and $k_{D,obs}$) were measured in triplicate. Reported errors are the standard errors of the mean. [b]Measured with initial rates

Table S4. Variation in VT-KIE parameters from kinetic experiments with different percent deuteration in the deuterated substrate.

Percent	Fluorene[a]		DHA	
Deuterated	$E_a(D) - E_a(H)$[b]	$\ln(A_H/A_D)$	$E_a(D) - E_a(H)$[b]	$\ln(A_H/A_D)$
0.95	1.0(3)	–0.2(5)	9(2)	–11(3)
0.96	1.0(3)	–0.2(5)	5.9(8)	–7(1)
0.97[c]	0.9(2)	–0.1(4)	4.5(4)	–4.5(7)
0.98[d]	0.9(2)	–0.1(4)	3.7(3)	–3.3(5)
0.99	0.8(2)	–0.1(4)	3.1(2)	–2.6(3)

The [a]See below for why we believe these parameters are less accurate than the ones from competition experiments. [b]kcal/mol [c]Best estimate of the percent deuteration in d_2-fluorene used. [d]Best estimate of the percent deuteration in the d_4-DHA used.

Analysis of the Yield of Competition Experiments

A yield of 17(3)% for five of the reactions at 263 K were determined by GC-MS, with 1.0 equivalents of *meta*-terphenyl as an internal standard include in the reactions (see Figure S1 and Table S5 and below). While this suggests caution must be taken in interpreting product isotope distributions, further considerations and experiments give us confidence in our conclusions based on the competition data.

By design our KIE determinations are resistant to being affected by side-reactions of fluorenyl radical. Because we measure the KIE with both (a) an intermolecular competition experiment between d_0-fluorene and d_2-fluorene and (b) an intramolecular competition C–H and C–D in d_1-fluorene, we can determine both the primary and secondary isotope effects separately. Promiscuous reactivity of fluorenyl radical may depend on the secondary isotope which is still present in the radical, but our results are based on the primary isotope effect which cannot have a direct influence on radical chemistry. In other words, in the intermolecular competition experiments, d_0-fluorenyl is produced by abstraction of an H-atom, so if there is selectively higher conversion of d_0-fluorenyl into bifluorenyl this will lead to an overestimation of k_H. However, in the intramolecular competition experiments d_0-fluorenyl is produced by abstraction of a D-atom, so the same overrepresentation of d_0-fluorenyl in the bifluorenyl product will instead result in an underestimation of k_H relative to k_D. The opposing effects on k_H manifests as a bias in the secondary isotope effect, not the primary isotope effect. For the primary isotope effect to be affected, the side reactivity would require an interaction between the fluorene substrate and the fluorenyl radical, such as self-exchange or scrambling of between the two. However, the rate of self-exchange between C–H bonds and radicals is too low for this to affect our experiments, see blow.

Nonetheless, despite the robust experimental design, we sought to test the reliability of our KIEs by perturbing reaction conditions (Figure S2 and Table S6). Running the competition experiments at 296 K in THF, at a higher concentration, and in the presence 10 equivalents of TEMPO had no effect on the observed deutration of the bifluorenyl product. This is especially of note in the reactions run with TEMPO, because these reactions had higher yields as determined with an anthracene internal standard (we believe TEMPO is acting as a radical scavenger and thereby mitigating side reactivity). Overall then, it is clear that while side-reactivity of the radical is taking place, all available evidence and considerations suggest this is not affecting our KIE data nor our conclusions from this study.

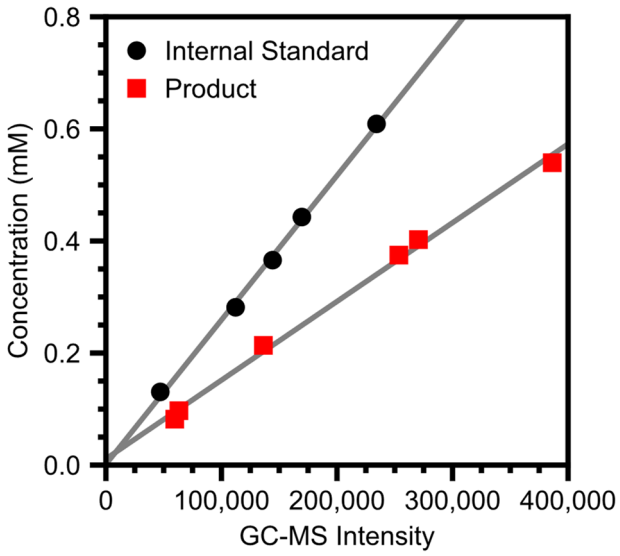

Figure S1. Calibration curves for GC-MS yields in DCM (toluene samples are dried and the GC-MS run with DCM, which is gentler on the instrument). The internal standard was *meta*-terphenyl, and the product bifluorenyl.

Table S5. Yields of reactions run at 263 K

Trial	Internal Standard	Product	
	Concentration (mM)	Concentration (mM)	Yield
1	0.556(6)	0.10(1)	17(2)%
2	0.441(5)	0.07(1)	16(2)%
3	0.452(5)	0.08(1)	18(2)%[b]

1 equivalent of *meta*-terphenyl was used as the internal standard. All errors propagated from the linear fits to calibration data. [a]Amount of internal standard not lost to transfer during workup.

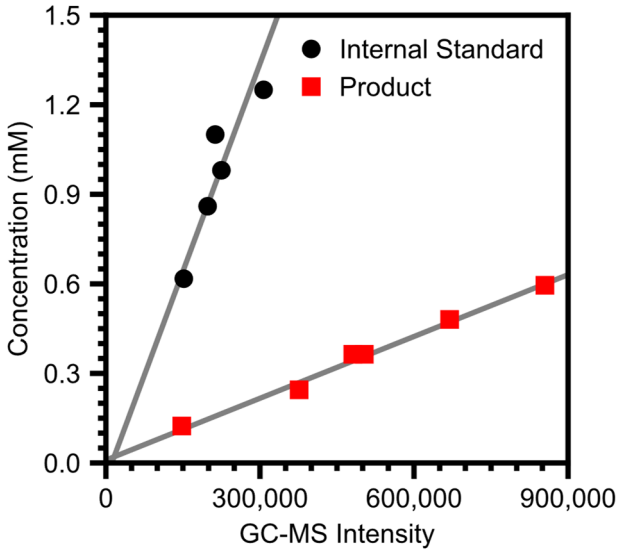

Figure S2. Calibration curves for GC-MS yields in THF. The internal standard was anthracene, and the product bifluorenyl. GC-maintenance and a change of solvent required new calibration curves. Due to perceived greater error in the intensity than in concentration, linear regression was done as intensity as a function of concentration to avoid attenuation bias in the calibration slope.

Table S6. Effect of Reaction Conditions on Yield and Product Deuteration

Change in Experimental Conditions	Yield[a]	p_D[b]	p-value[c]
1.25 mM in Toluene 20 equivalents d_1-fluorene[d]	N.D.[e]	72.7(6)%	N.D.[e]
1.25 mM in THF 20 equivalents d_1-fluorene	9.4%	73.5(1)%	0.29
2.27 mM in THF 100 equivalents d_1-fluorene	10.6%	73.80(6)%	0.29
25.0 mM in THF 40 equivalents d_1-fluorene	9.4%	73.5(4)%	0.29
1.25 mM in THF 20 equivalents d_1-fluorene 10 eq TEMPO additive	29%	73.47(7)%	0.29

Standard conditions are as described above, at 296 K. All reactions run as intramolecular competition with d_1-fluorene. 1 equivalent of anthracene was used as the internal standard. [a]Yield of bifluorenyl product. Propagated errors in the calibration curve are +/- 3–6%, but triplicate errors are +/- 2% or less. [b]Deuteration of bifluorenyl product. Errors are standard errors of the mean by a triplicate measurement. [c]Result from a two-tailed independent *t*-test of two populations assuming equal variances, with the null hypothesis that there is no change from standard conditions. [d]Standard conditions. [e]Not Determined.

Comparison of Competition and Kinetic KIE Data for Fluorene

Temperature dependent kinetic data for d_0-fluorene (k_H) and d_2-fluorene ($k_{D,obs}$) is shown in Figure S3. To check the consistency of this data with competition data, predicted $k_{D,obs}$ values were determined from k_H data and competition KIEs* as measured by GC-MS. These data are also shown in Figure S3. A summary of the data is given in Table S7. While the experimental and predicted k_D values are close, the differences have a notable effect on the KIE trends. The kinetic data suggest a substantially more temperature sensitive KIE ($E_a(D) - E_a(H) = 0.9(2)$) which results in a negative estimate of $\ln(A_H/A_D) = -0.1(4)$. This raises the question of which data set, competition or kinetic, is correct. We strongly believe that the competition data is less prone to systemic error and more trustworthy because (a) the plot of ln(KIE) vs. 1/RT from kinetic data has unusual curvature and (b) competition experiments are less sensitive to background reactivity not accounted for in our modelling.

Figure S3 shows the KIE values obtained from both competition experiments and kinetic experiments along with linear fits to the data. There is apparent curvature in the KIEs from kinetic experiments but not the KIEs from competition experiments. An *F*-test indicates that including a quadratic term in the fit of ln(KIE) vs. 1/RT significantly improves the fit to KIEs from kinetic experiments, giving a *p*-value of 0.0097 (with the null hypothesis of no change in the error when a quadratic term is added to the regression and the alternative hypothesis that addition of a quadratic term decreases the error). The same *F*-test with KIEs from competition experiments gives a *p*-value of 0.63. The positive curvature in ln(KIE) from kinetic data could be explained within semiclassical theory as the onset of tunneling across the temperature ranges studied. This onset would be expected to be caused by a reduction in the temperature sensitivity of k_H at lower temperature, i.e. positive curvature in ln(k_H) vs. 1/RT; less or no curvature would be expected in ln(k_D) vs. 1/RT.[5,6] However, this is not observed in our data; the same *F*-test for curvatures gives $p = 0.30$ for ln(k_H) and $p = 0.060$ for ln($k_{D,corr}$). The curvature is only significant at the $\alpha = 0.05$ level once k_H and k_D are compared, and if the curvature can be attributed to either of the data sets alone it would mostly likely be k_D, not k_H. This suggests the source of the curvature in KIEs from kinetic data is not the onset of tunneling within a semiclassical framework. We believe instead that the curvature is due to artifacts in the kinetic data, which leads us to conclude that the KIEs from competition experiments are more reliable.

A potential source for these artifacts is background reactivity which affect the UV-vis traces but the product ratios of the bifluorenyl product. That there is background reactivity in the kinetic reactions is demonstrated in Figure S5, a kinetic run of d_0-fluorene at 323 K run past completion. After the reaction is clearly completed, there is slight bleaching of the signal, as could be expected of a sensitive transition metal complex. However, this slight bleaching causes a monoexponential fit to underestimate the rate of reaction because the reaction appears to continue

* Expected $k_{D,obs} = p_0 k_H + \frac{1}{2} p_1 \frac{k_H}{KIE^{1\circ}} + \frac{1}{2} p_1 \frac{k_H}{KIE^{2\circ}} + p_2 \frac{k_H}{KIE^{1\circ} KIE^{2\circ}}$ with $KIE^{1\circ}$ the primary isotope effect and $KIE^{2\circ}$ the secondary isotope effect and $p_1 = 0.0284$, $p_2 = 0.0472$, and $p_3 = 0.9244$ being the proportions of d_n-fluorene as determined by GC-MS.

for longer than it really does (see the variation in the calculated k_{obs} value depending on which time point is used as the endpoint, Figure S5). Unless there is a coincidence, one would expect this bleaching to affect the rate differently at different temperatures and result in a slight bias to the measured activation energy and a larger bias to the extrapolated intercept. Further evidence for background reactivity is in our moderate product yields (17(3)%, see Table S5) which indicate fluorenyl radicals are engaging in side reactivity other than dimerization. It is plausible this side reactivity affects the absorbance at 470 nm; this would bias the measured k_{obs}. The competition experiments, however, directly measure the relative amount of d_0-fluorenyl and d_1-fluorenyl as recorded in the bifluorenyl product. This selectively analyzes the relative formation of different isotopomers of fluorenyl. If side reactivity results in an isotope dependence on conversion of fluorenyl to bifluorenyl, this would affect the measured secondary kinetic isotope effect, not the primary isotope effect. By performing both intramolecular and intermolecular competition experiments we were able to distinguish between primary and secondary effects.

Ultimately, the deviations between the two sets of data points is slight. Differences between the predicted and experimental values of $k_{D,obs}$ is primarily found at lower temperatures. This difference is greater than the precision of the measurement, but plausibly less than the accuracy of a kinetic measurement that is nonspecific to Co complexes being analyzed. The slight curvature in kinetically derived KIEs further suggests that the low-temperature kinetics are slightly suspicious, and cannot be trusted with the accuracy needed to confidently extrapolate to 1/kT = 0. Therefore, we believe the competition experiments give an accurate estimate of $\ln(A_H/A_D)$, as presented in the main text.

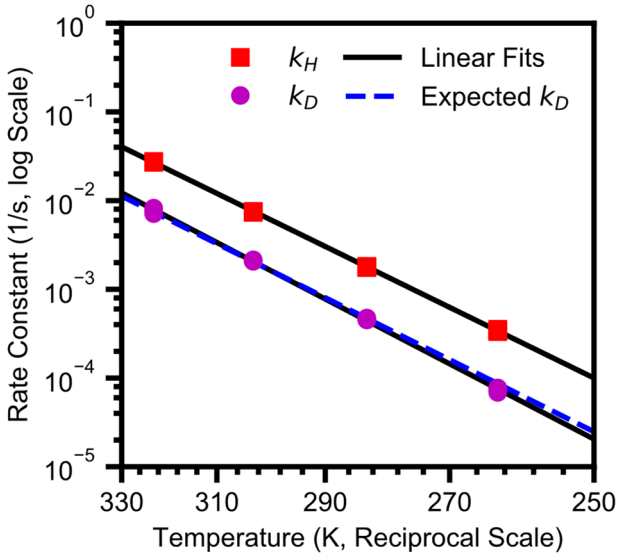

Figure S3. Plot of experimental k_H and $k_{D,obs}$ vs. 1/RT for the reaction of **CoO** with fluorene, with the corresponding linear fits shown in black. The predicted values of $k_{D,obs}$ determined from competition KIEs are shown in the blue dashed line (Table S7).

Table S7. Comparison of $k_{D,obs}$ measured by kinetics and expected from competition KIEs.

Temperature (K)	Expected $k_{D,obs}$ (s^{-1})	Experimental $k_{D,obs}$ (s^{-1})
323	$7.4 \cdot 10^{-3}$	$7.7(3) \cdot 10^{-3}$
303	$2.1 \cdot 10^{-3}$	$2.10(3) \cdot 10^{-3}$
283	$4.7 \cdot 10^{-4}$	$4.60(7) \cdot 10^{-4}$
263	$8.6 \cdot 10^{-5}$	$7.3(2) \cdot 10^{-5}$

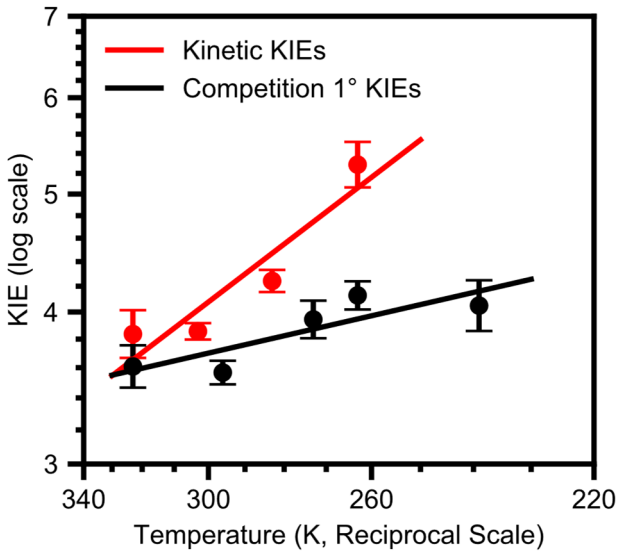

Figure S4. Plot of ln(KIE) vs. 1/RT for both KIEs from kinetic data and KIEs from competition data.

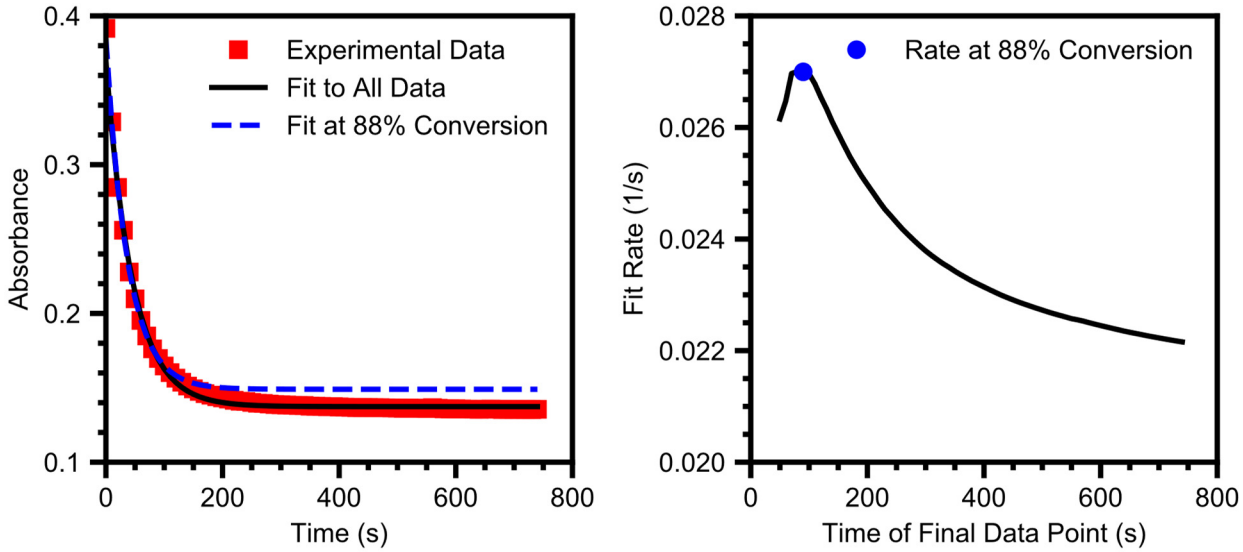

Figure S5. Absorbance at 470 nm for a reaction run past completion (left) and the dependency of k_{obs} on the reaction time (right).

Simulations of Scrambling in Competition Experiments

Our reliance on KIEs from competition data requires that any side reactivity of fluorenyl radical affects only the secondary KIE. However, it is possible for the primary KIE to be affected if self-exchange of H/D-atoms between fluorenyl and fluorene ("scrambling") is competitive with dimerization. For the intermolecular competition experiments with 1:1 d_0-fluorene:d_2-fluorene it would be expected that scrambling with d_0-fluorene is quicker than scrambling with d_2-fluorene, converting d_1-fluorenyl into d_0-fluorenyl. As d_0-fluorenyl is the product from C–H activation, this would result in a larger KIE (Scheme S2). For the intramolecular competition experiments with d_1-fluorenyl, the faster exchange of H-atoms than D-atoms would instead convert d_0-fluorene into d_1-fluorene, again converting C–D oxidation into apparent C–H oxidation with a higher corresponding KIE. However, the reported rate constants for self-exchange of organic radicals are orders of magnitude slower than the reported rate constants for dimerization.[7,8] Nonetheless, it is nontrivial to compare the rate constants of a reaction second order in radical (dimerization) with a rate constant first order in radical (scrambling), so we performed numerical simulations to confirm that this orders of magnitude difference is sufficient.

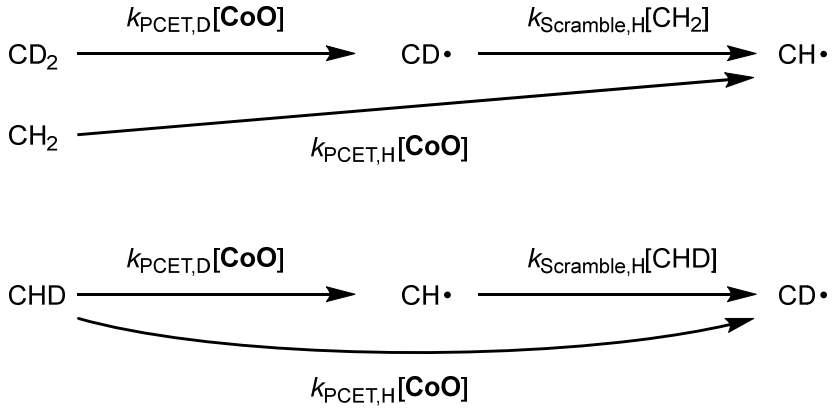

Scheme S2. How self-exchange could convert C–D oxidation into apparent C–H oxidation.

Kinetic modelling was done via numerical integration using python. For each reaction in Scheme S3, an instantaneous rate was determined for a given concentrations of each reagent. The contribution of all reactions on the individual reagents and products was summed to give an instantaneous rate of change in each species' concentration, which allows an estimate of the concentrations at a slightly later time. Concentrations were integrated from initial concentrations of 0.00125 M **CoO** and 0.0125 M each of CH_2 and CD_2 (as in our intermolecular competition experiments; all other initial concentrations 0) using the LSODA method implemented in scipy. The values of k_{PCET} and KIE_{PCET} were set at 2.3 and 4, respectively, as determined by experiment. The value of $KIE_{scramble}$ was set to 100 to represent an extreme case.

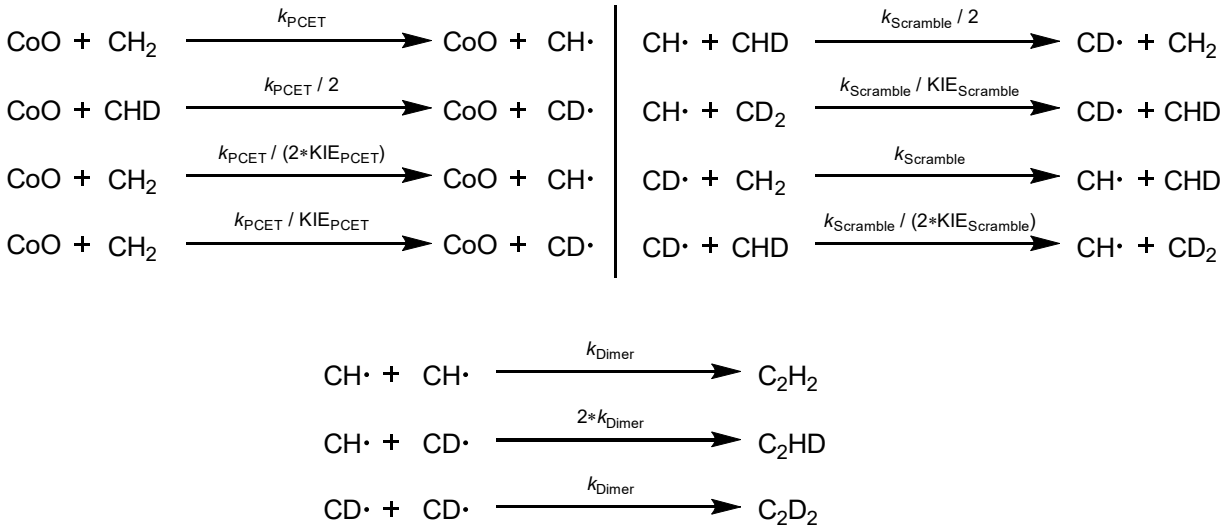

Scheme S3. Reactions and corresponding rate constants simulated to analyze the effect of scrambling.

Figure S6 shows the results of these simulations for both the expected low value of $k_{Scramble} = 10^{-10}$ $M^{-1}s^{-1}$ and the unrealistically large value of $k_{scramble} = 10^{-1}$ $M^{-1}s^{-1}$ (the self-exchange rate of toluene, ~10^{-4} $M^{-1}s^{-1}$, is a more realistic upper bound but is visually indistinguishable from the lower expected value).[7] Literature suggests that k_{Dimer} is expected to be ~10^{10} $M^{-1}s^{-1}$, but we examined values as low as 1 $M^{-1}s^{-1}$.[8] Even with the unrealistically large rate of self-exchange, an unrealistically low rate of dimerization is necessary to have a noticeable impact in the measured KIE. Therefore, the ~20 orders of magnitude separating the dimerization rate constants and self-exchange rate constants are plenty to ensure our competition experiments are unaffected by scrambling.

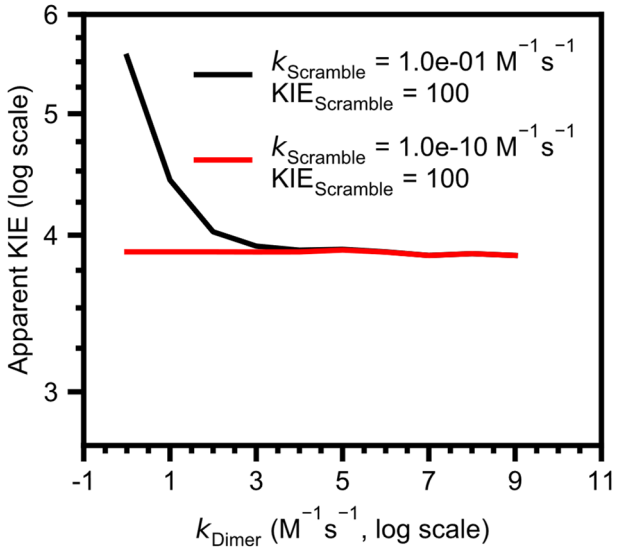

Figure S6. The apparent KIEs simulated for an actual KIE of 4 affected by the self-exchange of fluorenyl radical with fluorene.

Simulations of KIEs Within a Semiclassical Context

To demonstrate how the positive $\ln(A_H/A_D)$ is unexplainable within a semiclassical context, we fit the observed $E_a(D) - E_a(H)$ and $\ln(A_H/A_D)$ values to semiclassical Eckart barriers with a tunneling correction and show that the barriers needed to obtain a positive $\ln(A_H/A_D)$ are chemically implausible. Within a semiclassical framework the KIE can be modelled as:

$$KIE = \frac{Q_H(T)k_{H,S}}{Q_D(T)k_{D,S}} = \frac{Q_H(T)}{Q_D(T)}\left(\frac{A_H}{A_D}\right)_S e^{\frac{\left(E_a(D)-E_a(H)\right)_S}{RT}}$$

with the subscript S indicating semiclassical values (no tunneling) for the rates k_H and k_D, the Arrhenius prefactor ratio A_H/A_D, and the difference in activation energies $E_a(E) - E_a(H)$. Q_H and Q_D are the tunneling corrections for the reactivity of H and D, respectively. These tunnelling corrections in turn are calculated from transmission coefficients of H and D integrated over various energies with each energy weighted according to temperature. See Bell for a more complete description of this framework for estimating semiclassical KIEs and their tunneling corrections, and Johnson and Heicklen for formula involving Eckart barriers in particular.[5,9] This then gives the temperature dependence in ln(KIE) as having a semiclassical slope and intercept modified by $\ln(Q_H(T)/Q_D(T))$:

$$\ln(KIE) = \ln\left(\frac{Q_H(T)}{Q_D(T)}\right) + \ln\left(\frac{A_H}{A_D}\right)_S + \frac{1}{RT}\left(E_a(D) - E_a(H)\right)_S$$

As the values of $\ln(Q_H(T)/Q_D(T))$ depend on the height and curvature of the barrier, the experimentally observed ln(KIE) can be used to determine a curvature and height, so long as assumptions can be made regarding the semiclassical values $\ln(A_H/A_D)_S$ and $(E_a(D) - E_a(H))_S$ and the barrier shape. Note that this "barrier height" does not need to equal the activation energy (or a hypothetical "no tunneling" activation energy), because some nuclear motions required for the reaction are not as susceptible to tunneling (e.g. rehybridization changes in bond lengths for the donor and acceptor). We use Eckart barriers, which is a typical choice in other studies.[10–12] Figure S7 shows the results of such simulations for fluorene competition KIEs, using Eckart barriers with a ΔE_{Rxn} of −3 kcal/mol and the mass of the proton/deuteron as the tunneling masses. Figure S8 show the same fit for DHA KIEs (ΔE_{Rxn} = −7 kcal/mol).

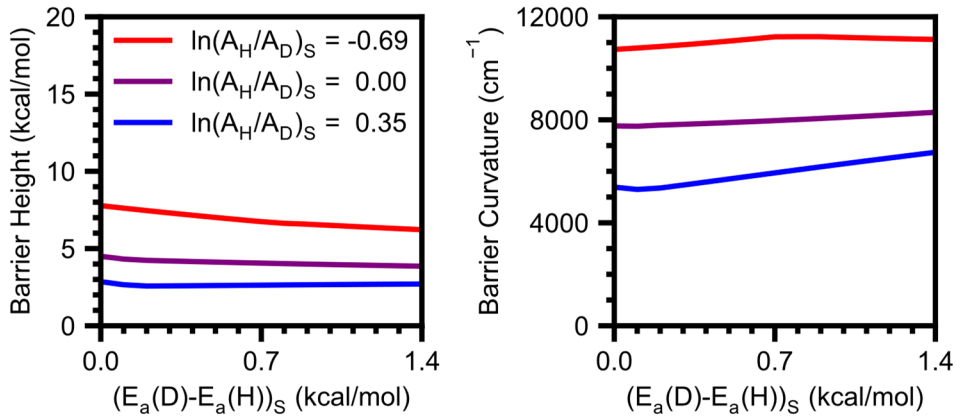

Figure S7. Simulated barrier heights (left) and curvature (right) for tunneling through an Eckart Barrier with ΔE_{rxn} = −3 kcal/mol resulting in the KIEs observed from fluorene competition experiments.

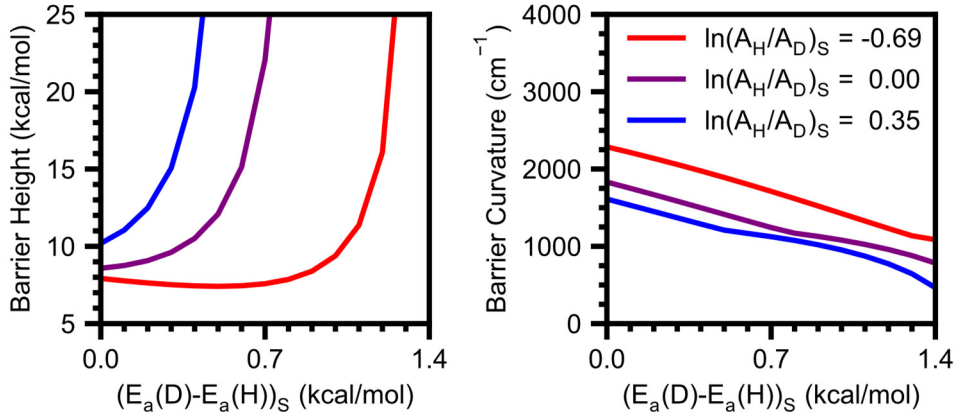

Figure S8. Simulated barrier heights (left) and curvature (right) for tunneling through an Eckart Barrier with ΔE_{rxn} = −7 kcal/mol resulting in the KIEs observed from DHA kinetic experiments. The y-axis is cut off at 25 kcal/mol to more clearly showcase the reasonable fits for certain values of $\ln(A_H/A_D)_S$.

These results are similar to those of Stern and Weston.[13] Essentially, to obtain an $\ln(A_H/A_D)$ as large as what is observed for fluorene, the transition state mode would need to have unreasonably sharp curvature, i.e. the barrier would need to be unreasonably thin. Transition states for metal-oxo mediated C–H activation typically lie within ~1,000-2,000 cm^{-1}, although slightly larger values are not unreasonable.[10–12] However, for the oxidation of fluorene by **CoO** the $\ln(A_H/A_D)$ observed from competition experiments would require transition state curvature substantially sharper than the curvature of stable covalent hydrogen bond (around 3,000 cm^{-1} for a C–H bond and somewhat larger for O–H bonds) which is chemically implausible. The highly temperature-dependent KIEs observed for DHA, however, are consistent with reasonable barrier curvature. Certain assumptions for semiclassical temperature dependence give implausibly high barriers, but other values have perfectly reasonable results.

While we chose ΔE_{Rxn} to closely match ΔG°_{CPET}, there is no reason this has to be the case for the same reason that the barrier height does not need to match the activation energy (also spin-

state dynamics could change the apparent ΔG°_{CPET}), Figure S9 shows a fit to fluorene competition KIE with $\Delta E_{Rxn} = -7$ kcal/mol with qualitatively the same results.

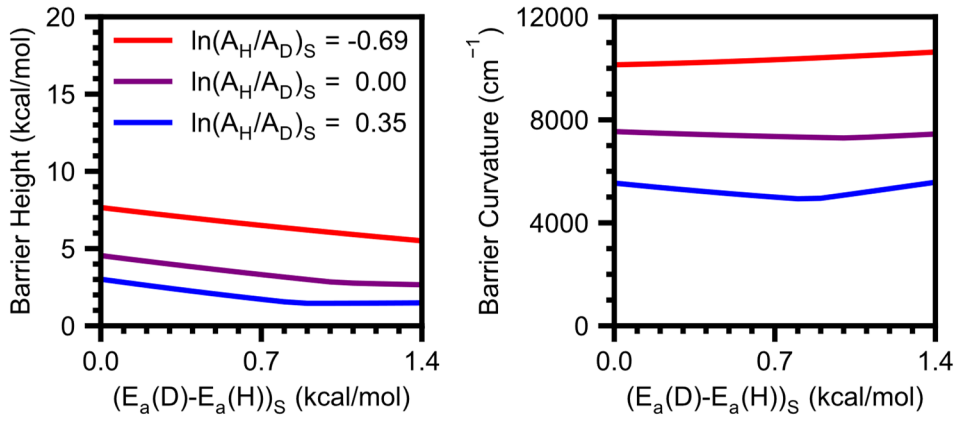

Figure S9. Simulated barrier heights (left) and curvature (right) for tunneling through an Eckart Barrier with $\Delta E_{rxn} = -7$ kcal/mol resulting in the KIEs observed from fluorene competition experiments.

Covariance Matrices of Arrhenius Parameters

Table S8, Table S9, and Table S10 give the covariance matrices of the fits to $E_a(D) - E_a(H)$ and $\ln(A_H/A_D)$. The diagonal entries are the variances of the fit, the off-diagonal entries are the covariances between different parameters.

Table S8. Variances and covariances for Arrhenius parameters of reactivity with fluorene fit to competition data.

	1° $E_a(D) - E_a(H)$ (kcal/mol)	1° $\ln(A_H/A_D)$	2° $E_a(D) - E_a(H)$ (kcal/mol)	2° $\ln(A_H/A_D)$
1° $E_a(D) - E_a(H)$ (kcal/mol)	0.0068026	-0.012325	0.0010725	-0.001938
1° $\ln(A_H/A_D)$	-0.012325	0.0225645	-0.001938	0.0035396
2° $E_a(D) - E_a(H)$ (kcal/mol)	0.0010725	-0.001938	0.0041682	-0.007565
2° $\ln(A_H/A_D)$	-0.001938	0.0035396	-0.007565	0.0138743

Table S9. Variances and covariances for Arrhenius parameters of reactivity with fluorene fit to kinetic data.

	$E_a(D) - E_a(H)$ (kcal/mol)	$\ln(A_H/A_D)$
$E_a(D) - E_a(H)$ (kcal/mol)	0.006174	−0.1066
$\ln(A_H/A_D)$	−0.1066	0.1852

Table S10. Variances and covariances for Arrhenius parameters of reactivity with DHA fit to kinetic data.

	$E_a(D) - E_a(H)$ (kcal/mol)	$\ln(A_H/A_D)$
$E_a(D) - E_a(H)$ (kcal/mol)	0.05836	−0.1008
$\ln(A_H/A_D)$	−0.1008	0.1751

GC-MS Spectra for Competition Experiments

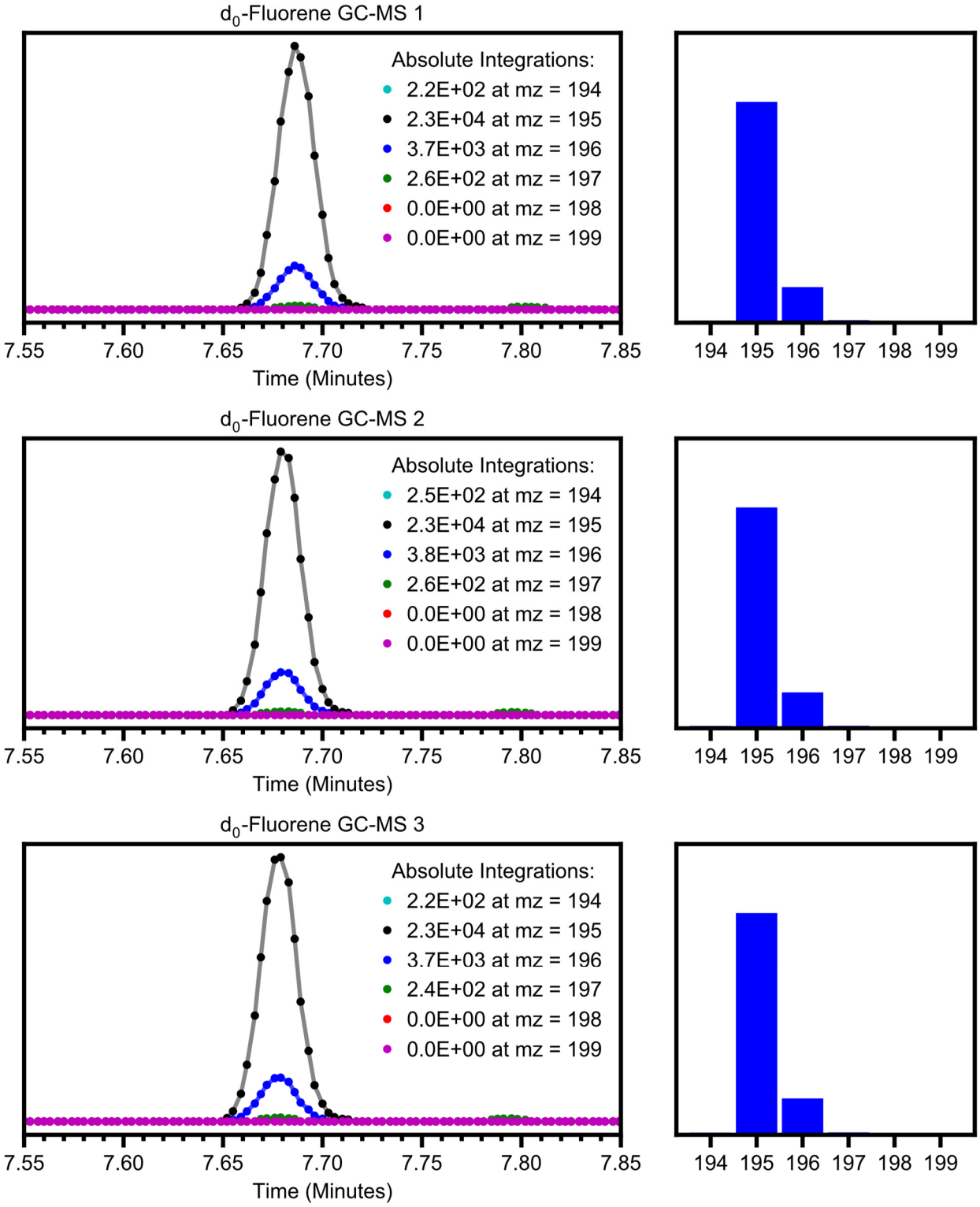

Figure S10. Reference GC-MS data for d_0-fluorene used for determining isotope composition of deuterated fluorene.

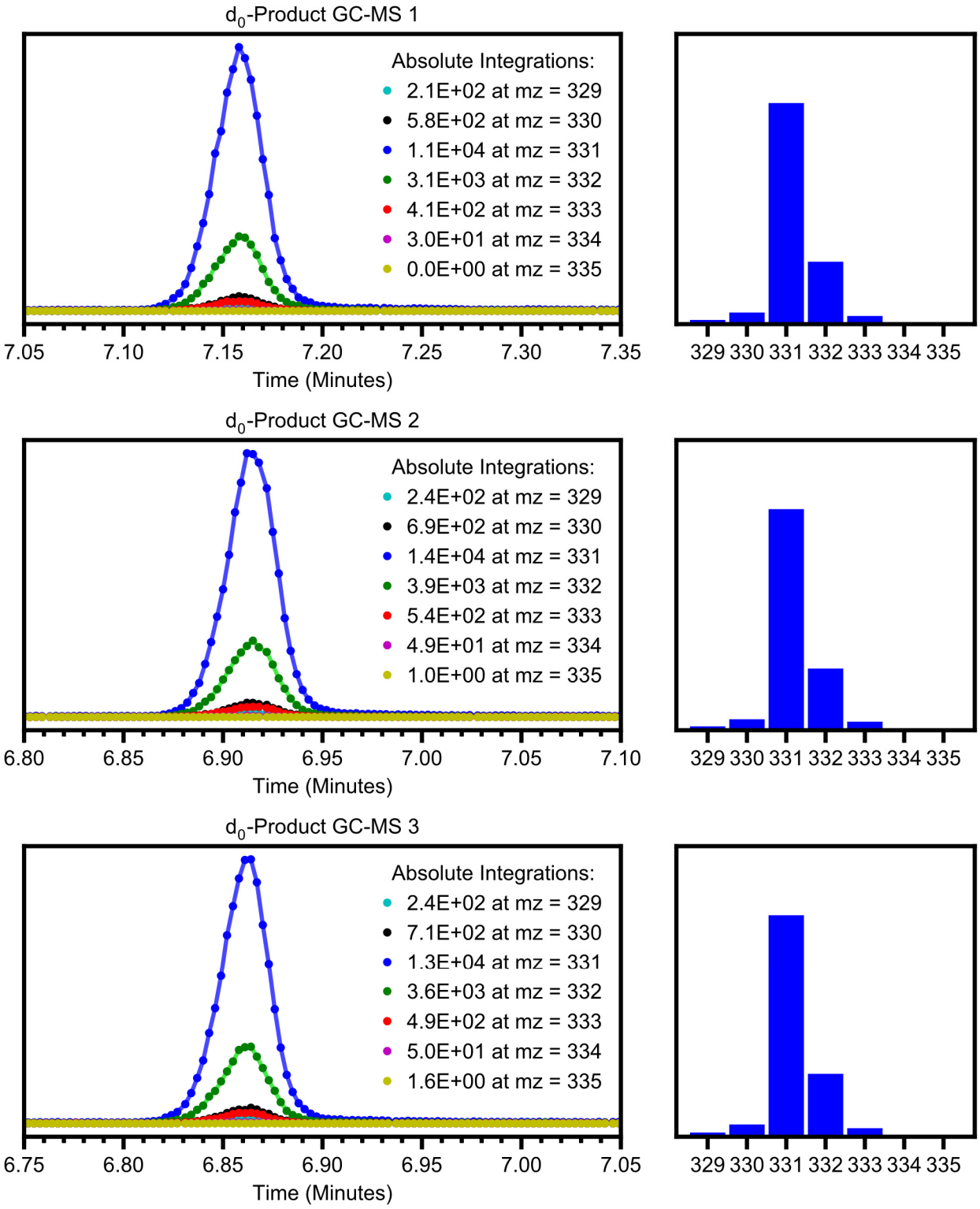

Figure S11. Reference GC-MS data for d_0-bifluorenyl used for determining isotope composition of deuterated bifluorenyl; sample prepared analogously to competition experiments but performed with d_0-fluorene.

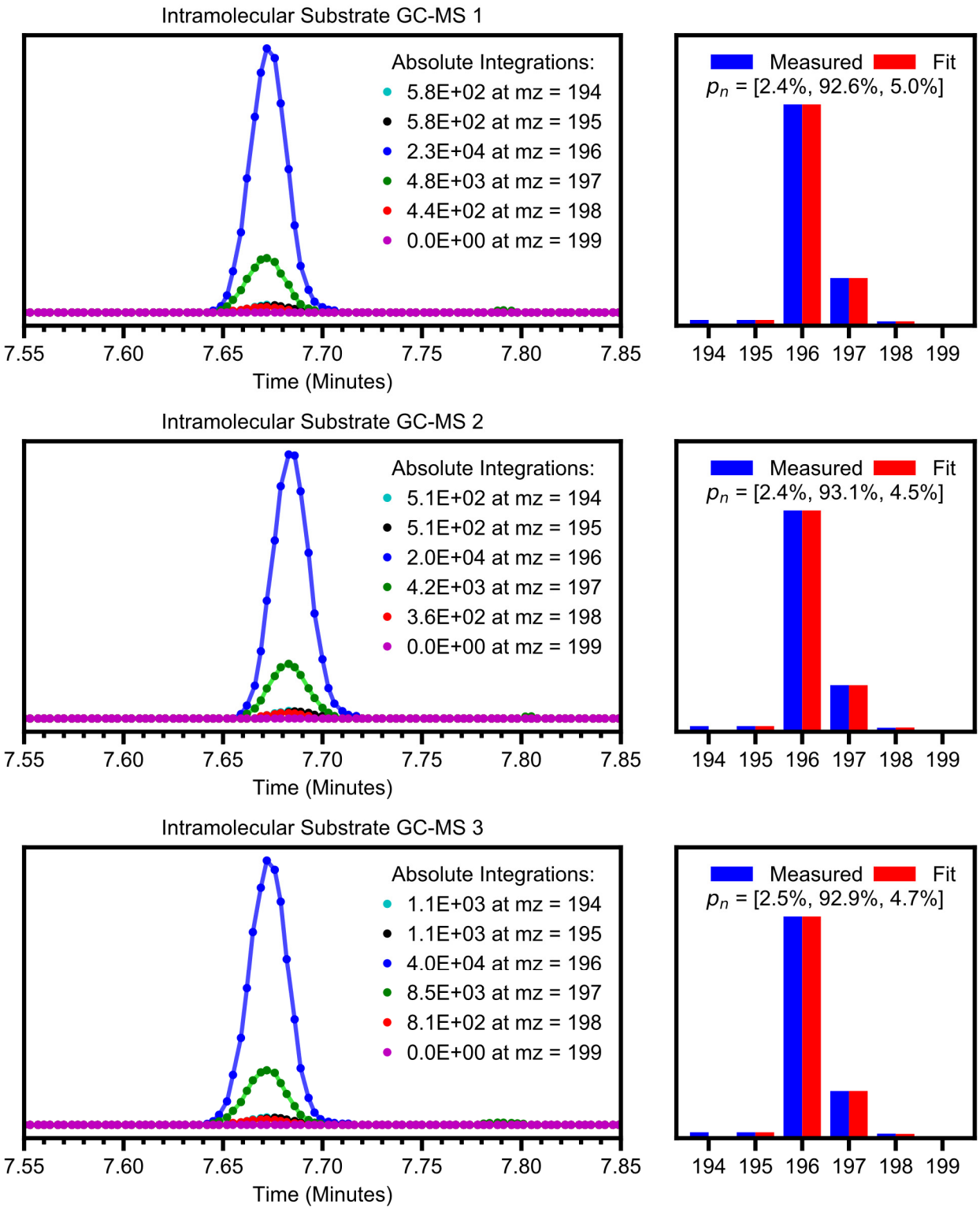

Figure S12. GC-MS data of mixture of d_1-fluorene used for intramolecular competition experiments.

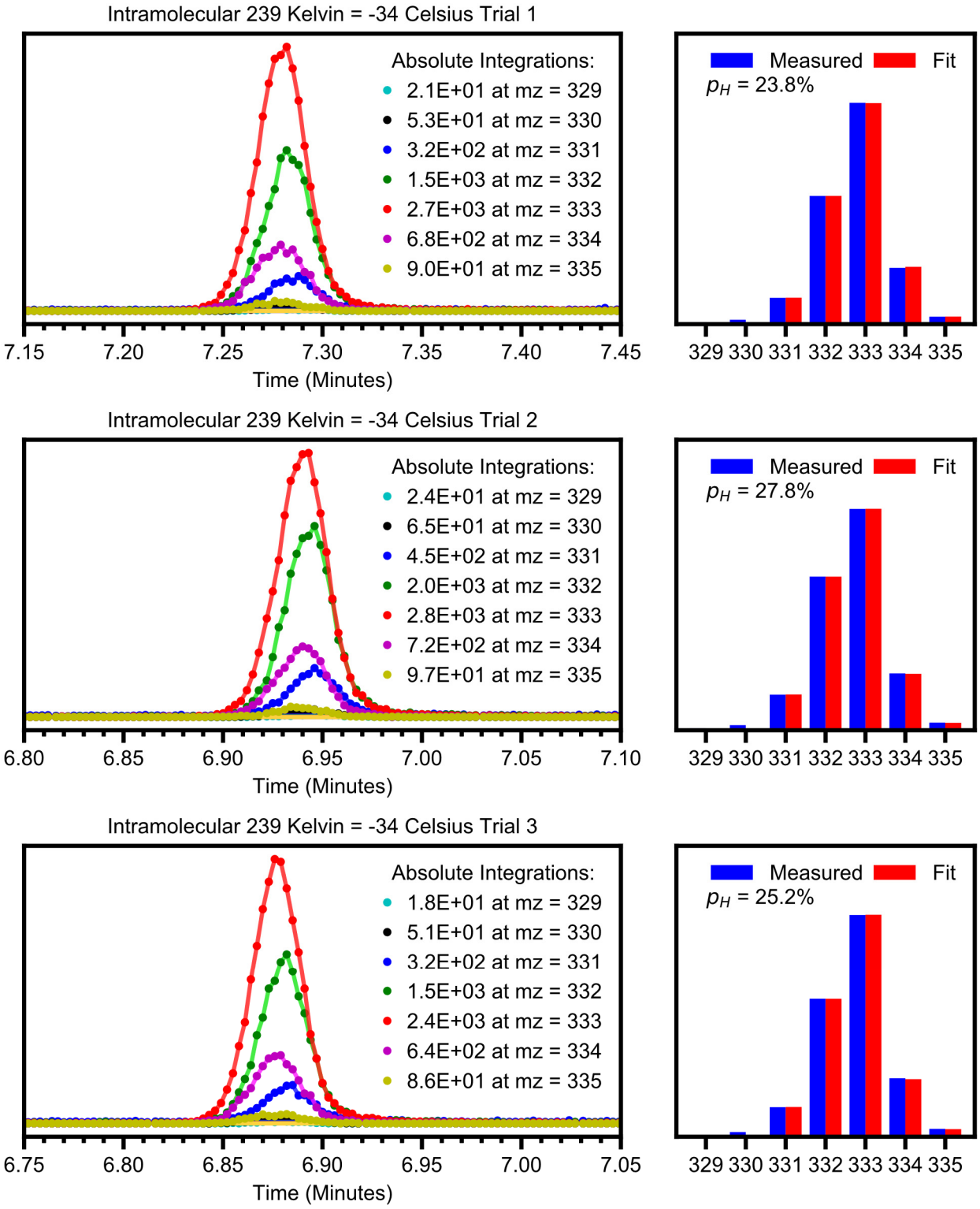

Figure S13. GC-MS data for the product analysis of the reaction of **CoO** and d_1-fluorene at 239 K.

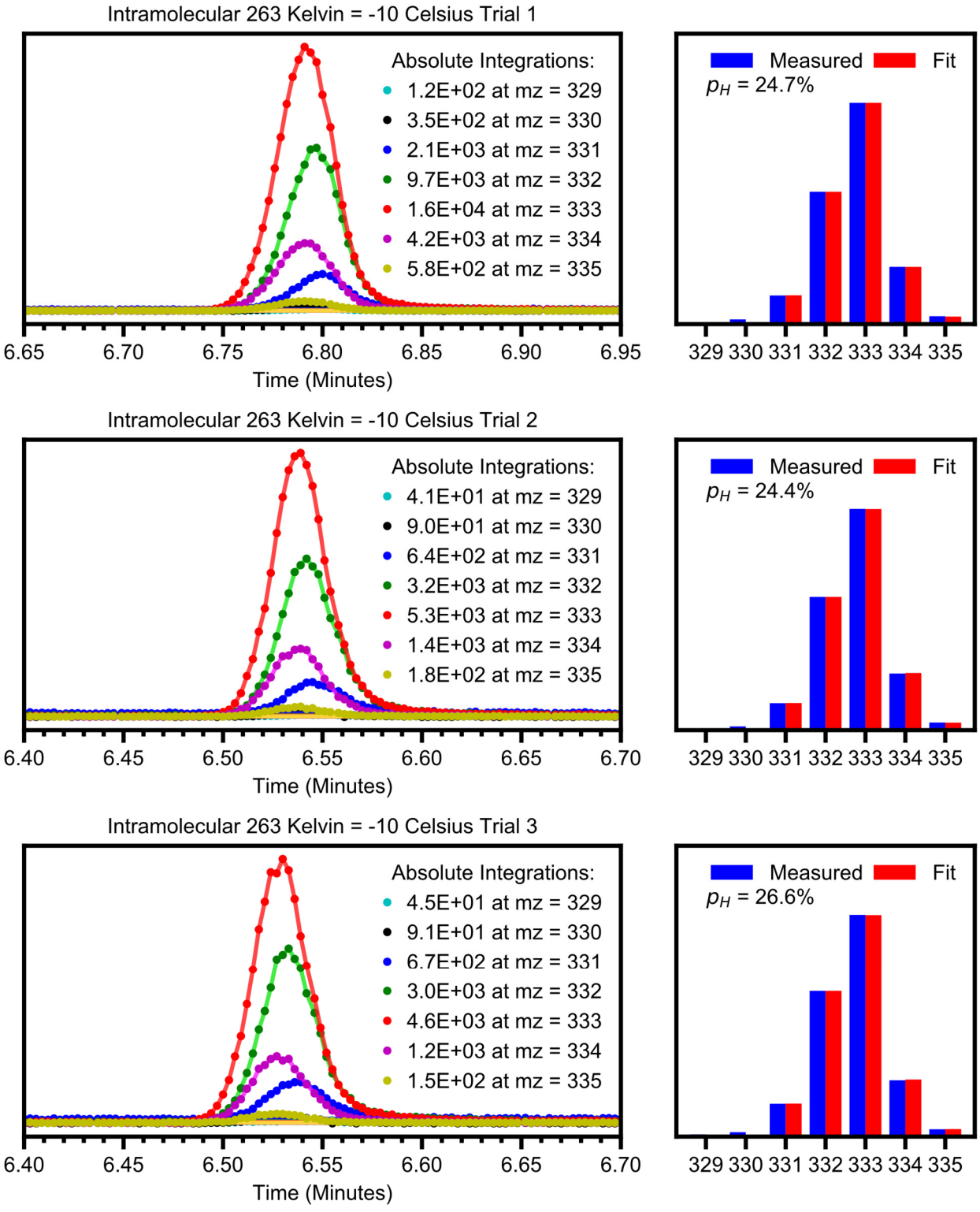

Figure S14. GC-MS data for the product analysis of the reaction of **CoO** and d_1-fluorene at 263 K.

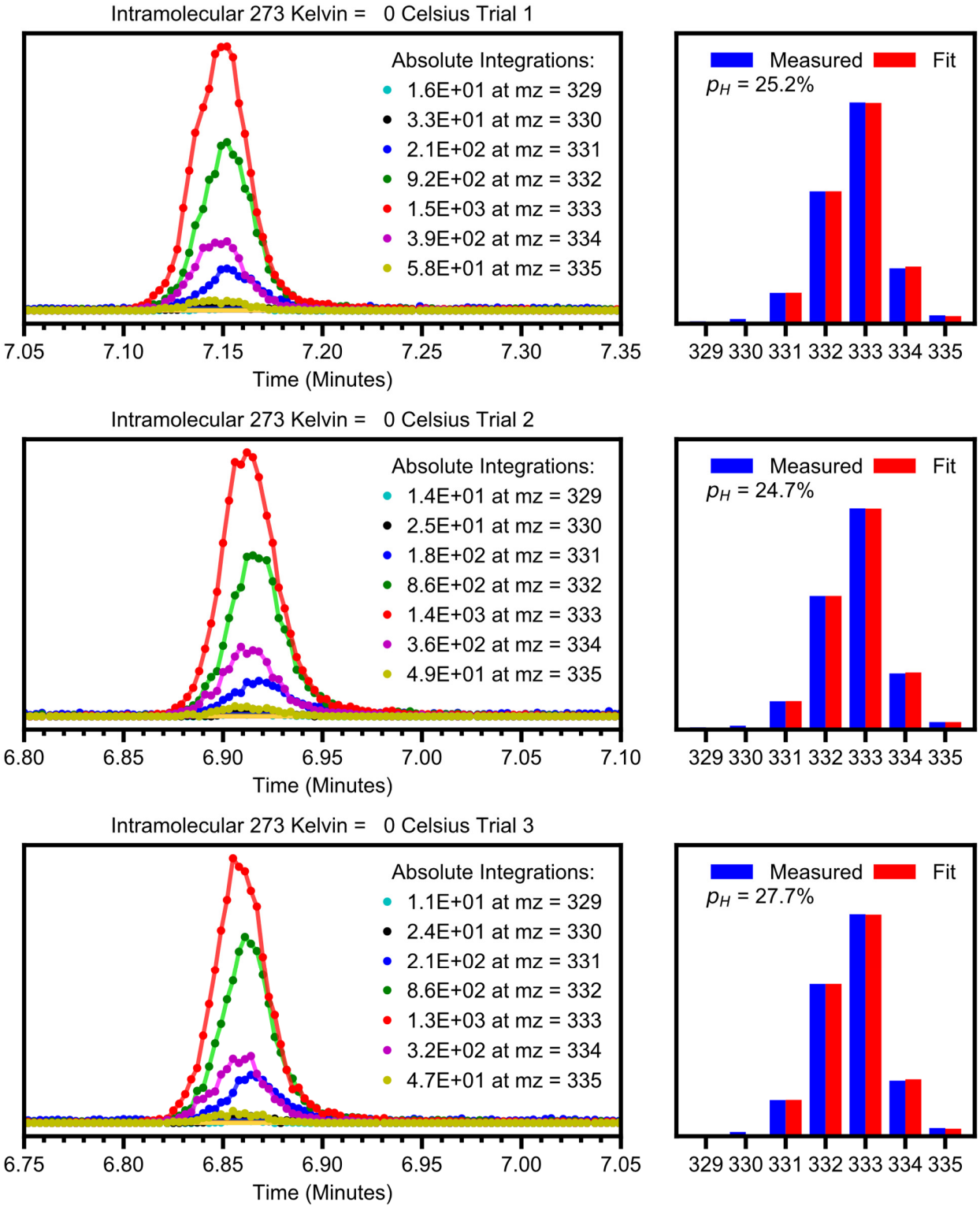

Figure S15. GC-MS data for the product analysis of the reaction of **CoO** and d_1-fluorene at 273 K.

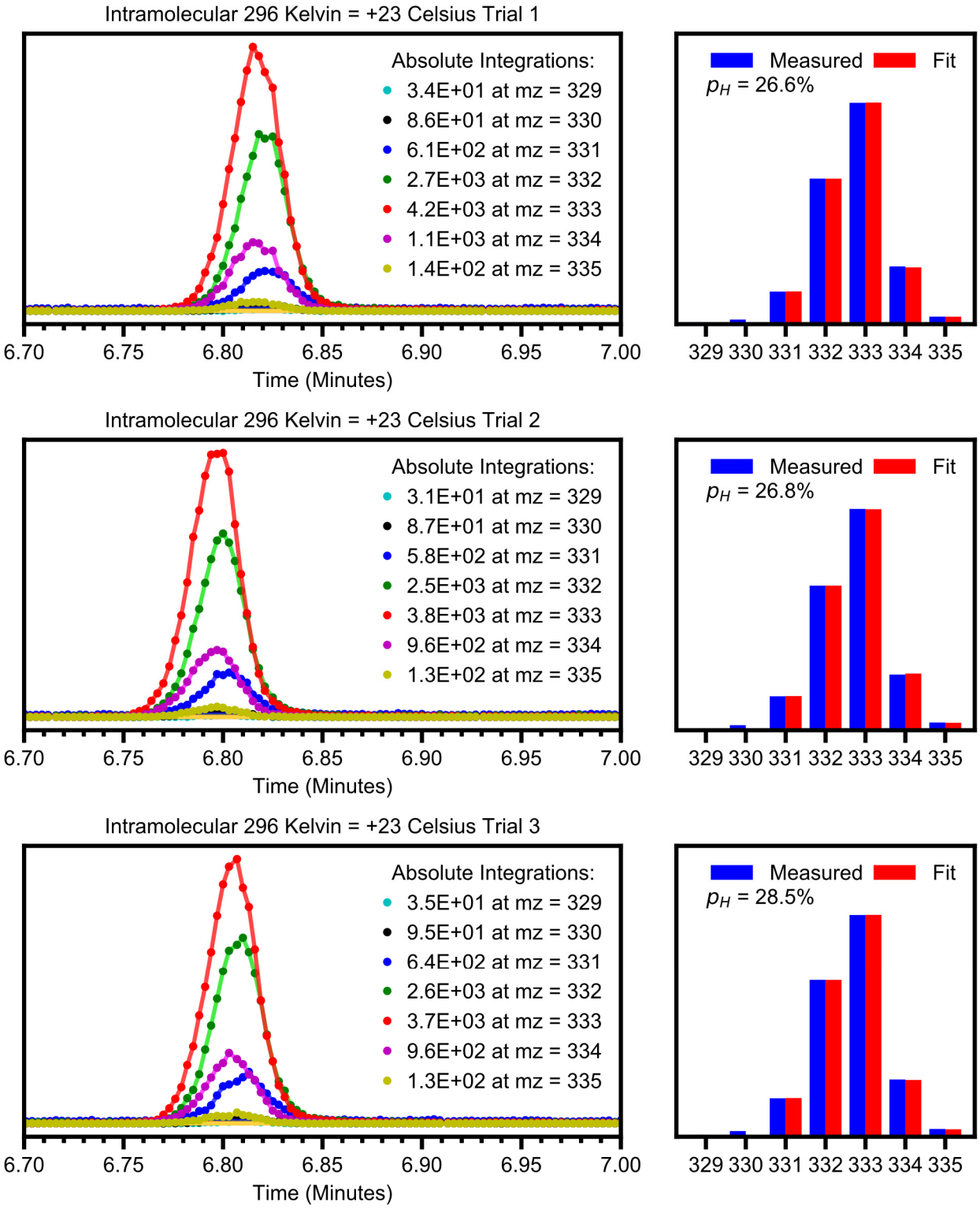

Figure S16. GC-MS data for the product analysis of the reaction of **CoO** and d_1-fluorene at 296 K.

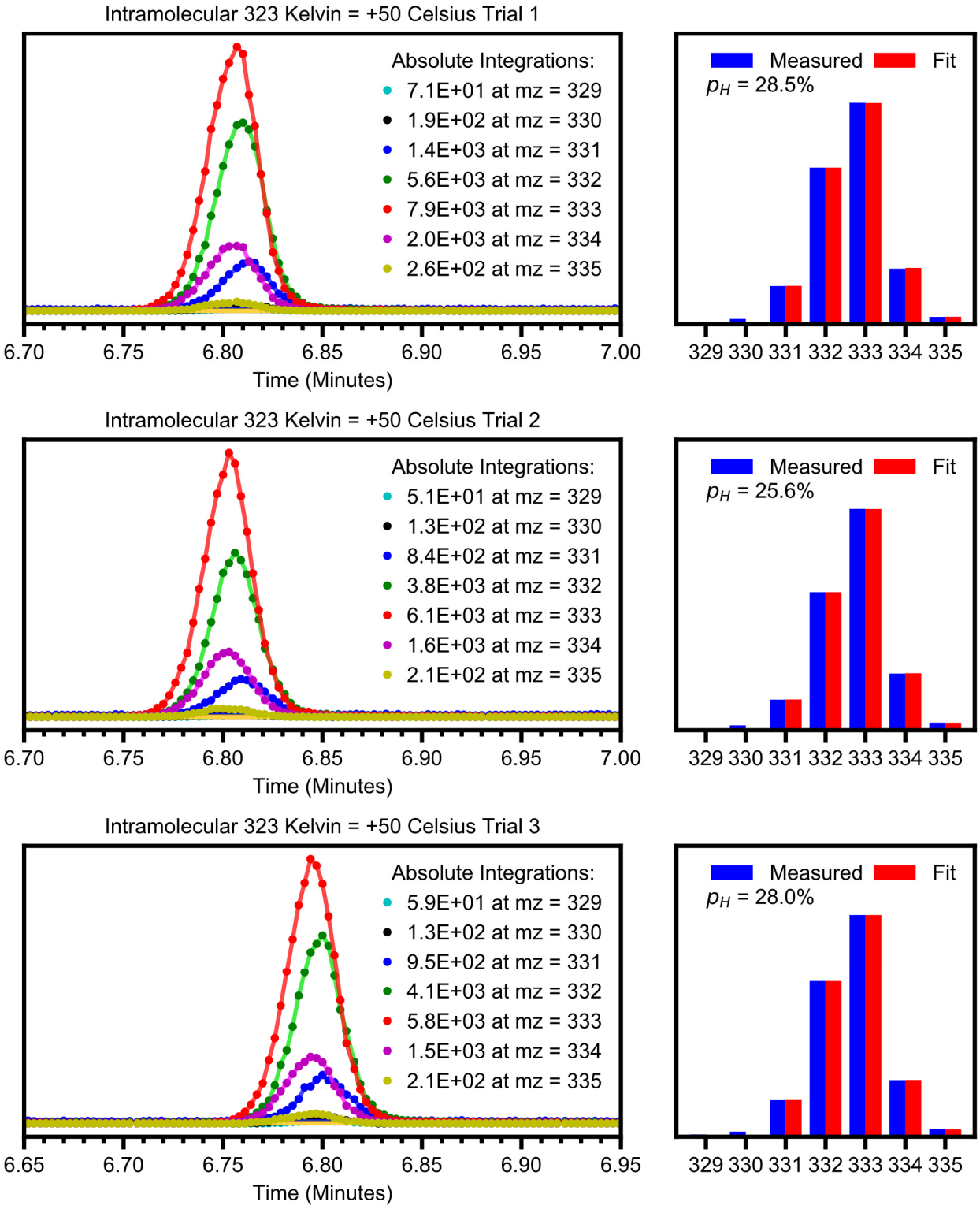

Figure S17. GC-MS data for the product analysis of the reaction of **CoO** and d_1-fluorene at 323 K.

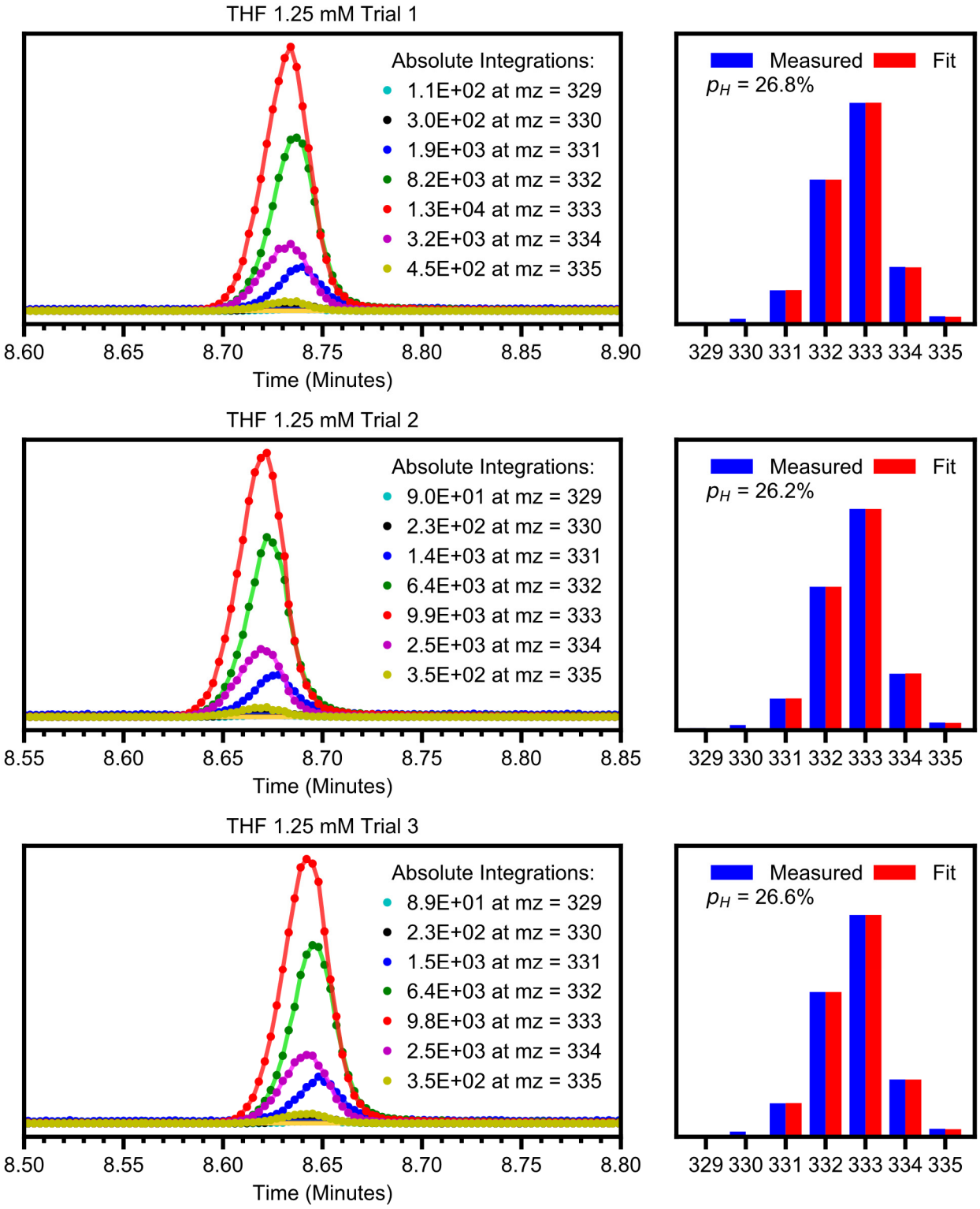

Figure S18. GC-MS data for the product analysis of the reaction of **CoO** and 20 equivalents d_1-fluorene at 296 K in THF at 1.25 mM **CoO**.

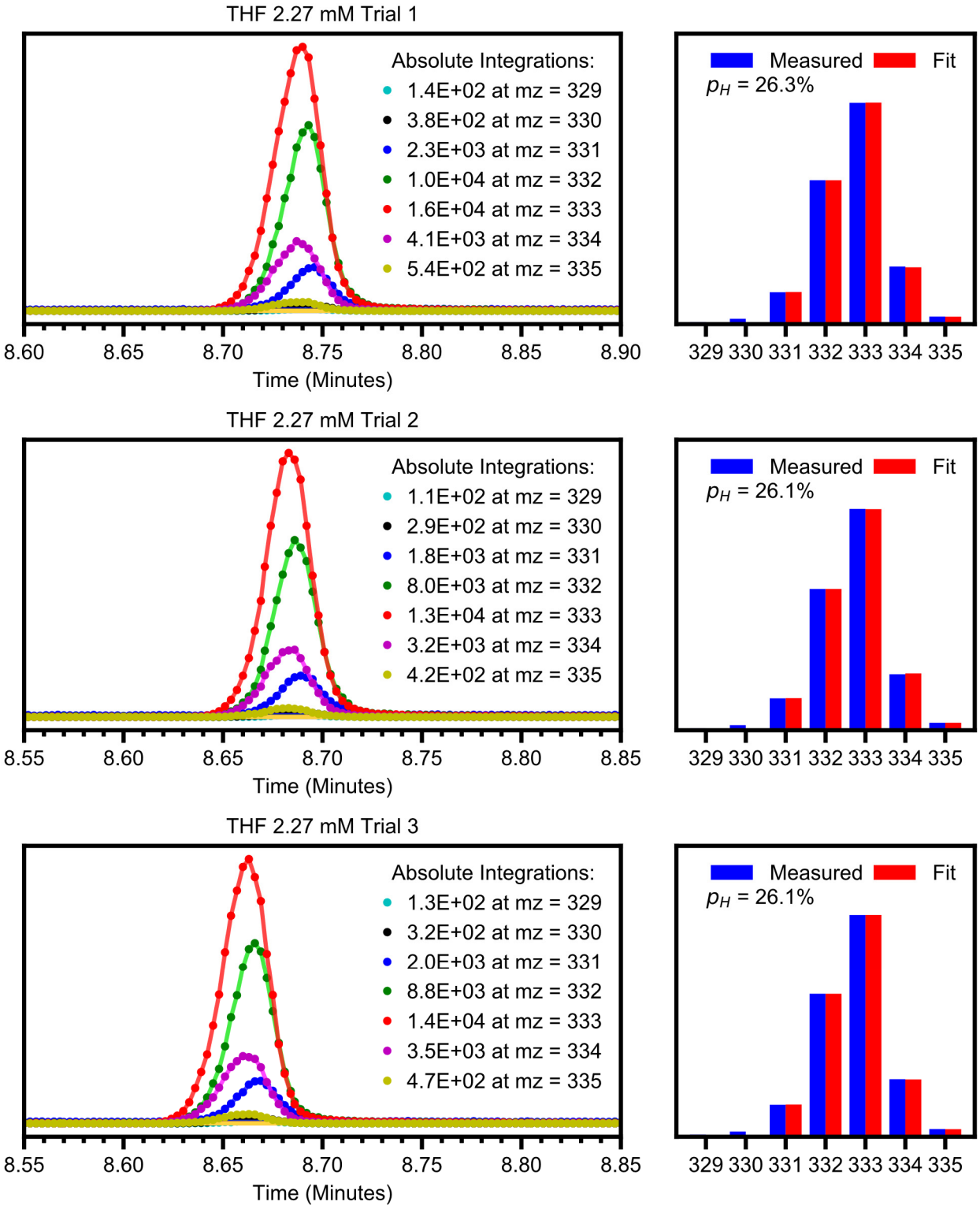

Figure S19. GC-MS data for the product analysis of the reaction of **CoO** and 100 equivalents d_1-fluorene at 296 K in THF at 2.27 mM **CoO**.

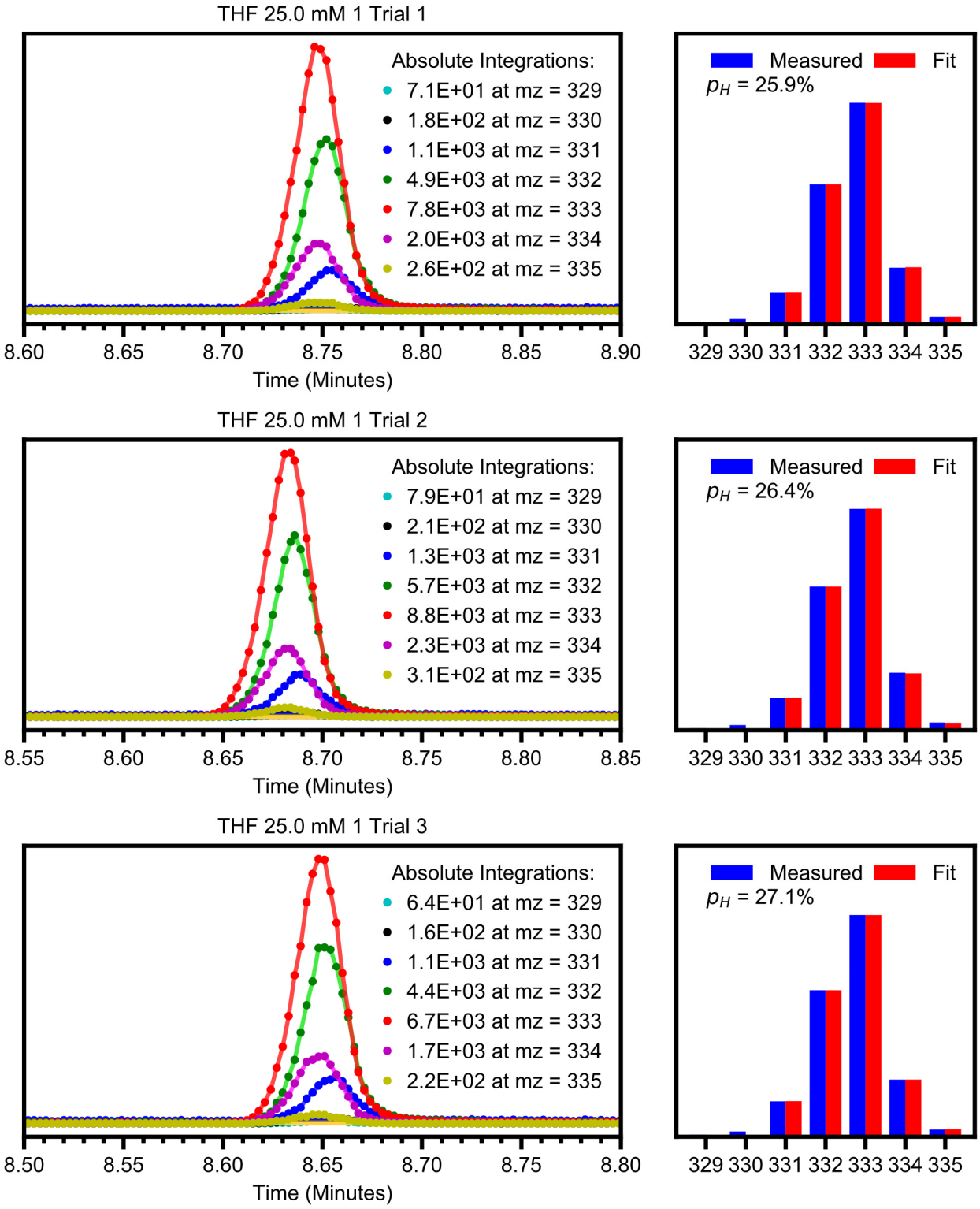

Figure S20. GC-MS data for the product analysis of the reaction of **CoO** and 40 equivalents d_1-fluorene at 296 K in THF at 25 mM **CoO**.

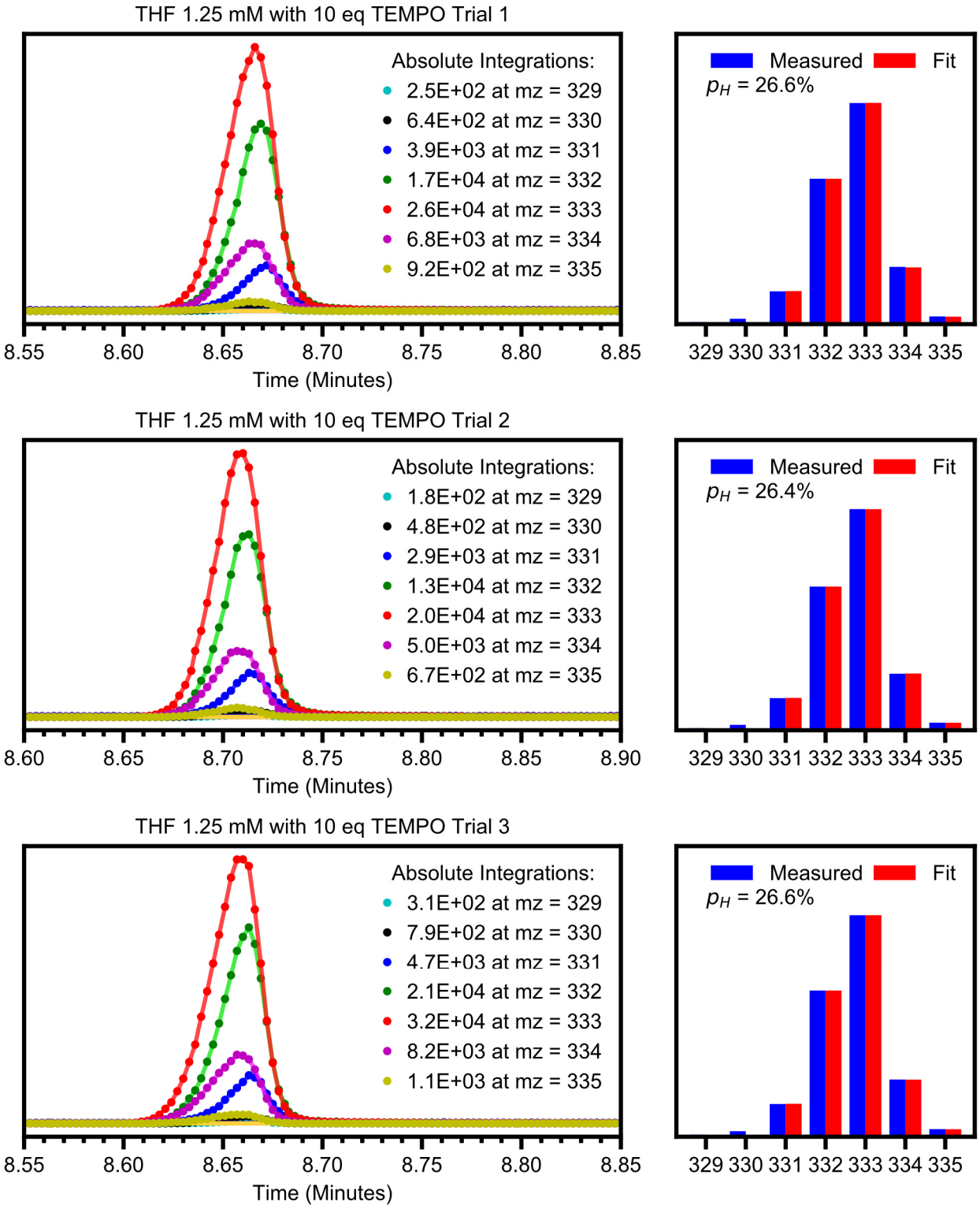

Figure S21. GC-MS data for the product analysis of the reaction of **CoO** and 20 equivalents d_1-fluorene at 296 K in THF at 1.25 mM **CoO** with an additive of 10 equivalents of TEMPO.

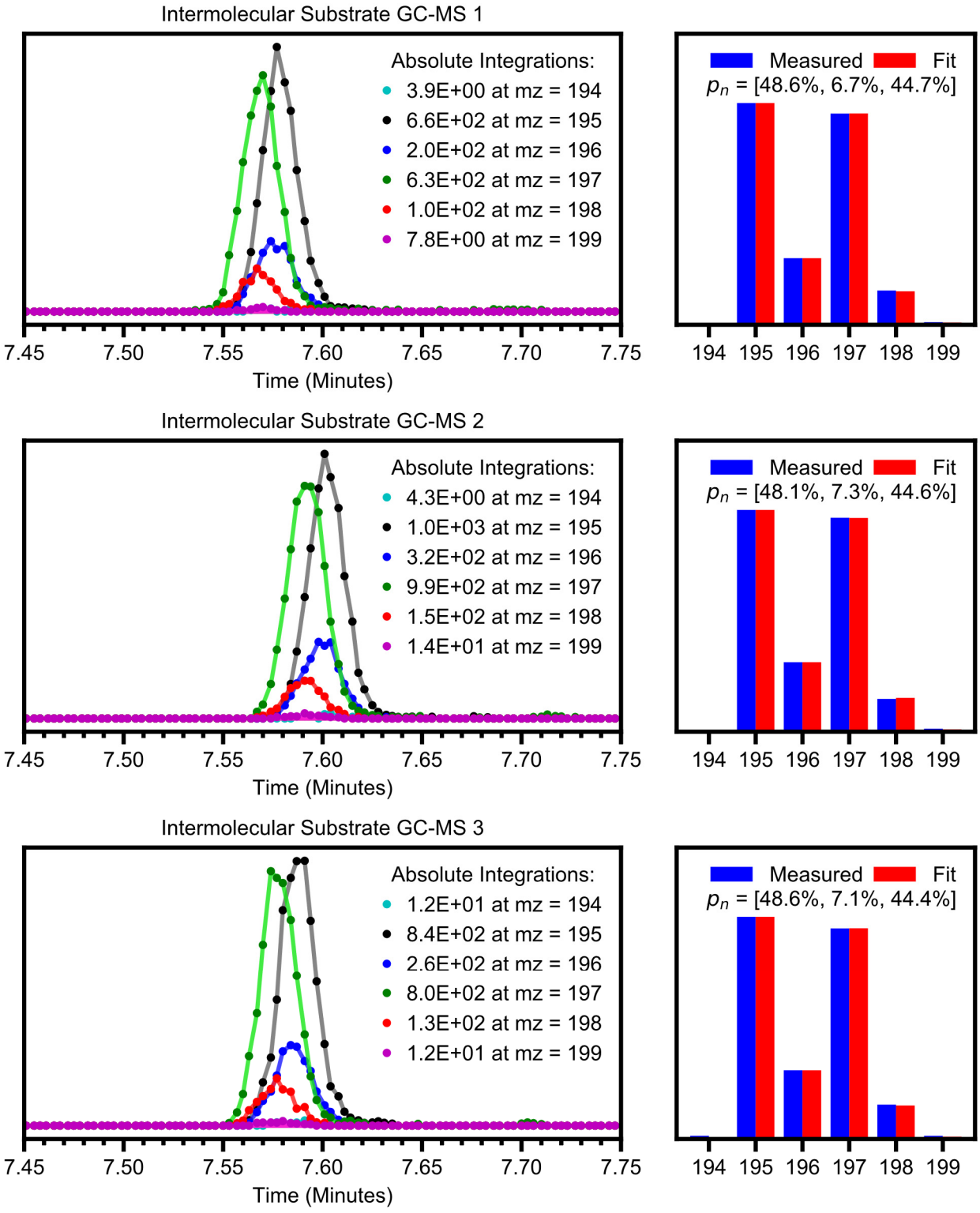

Figure S22. GC-MS data of mixture of d_0/d_2-fluorene used for intermolecular competition experiments.

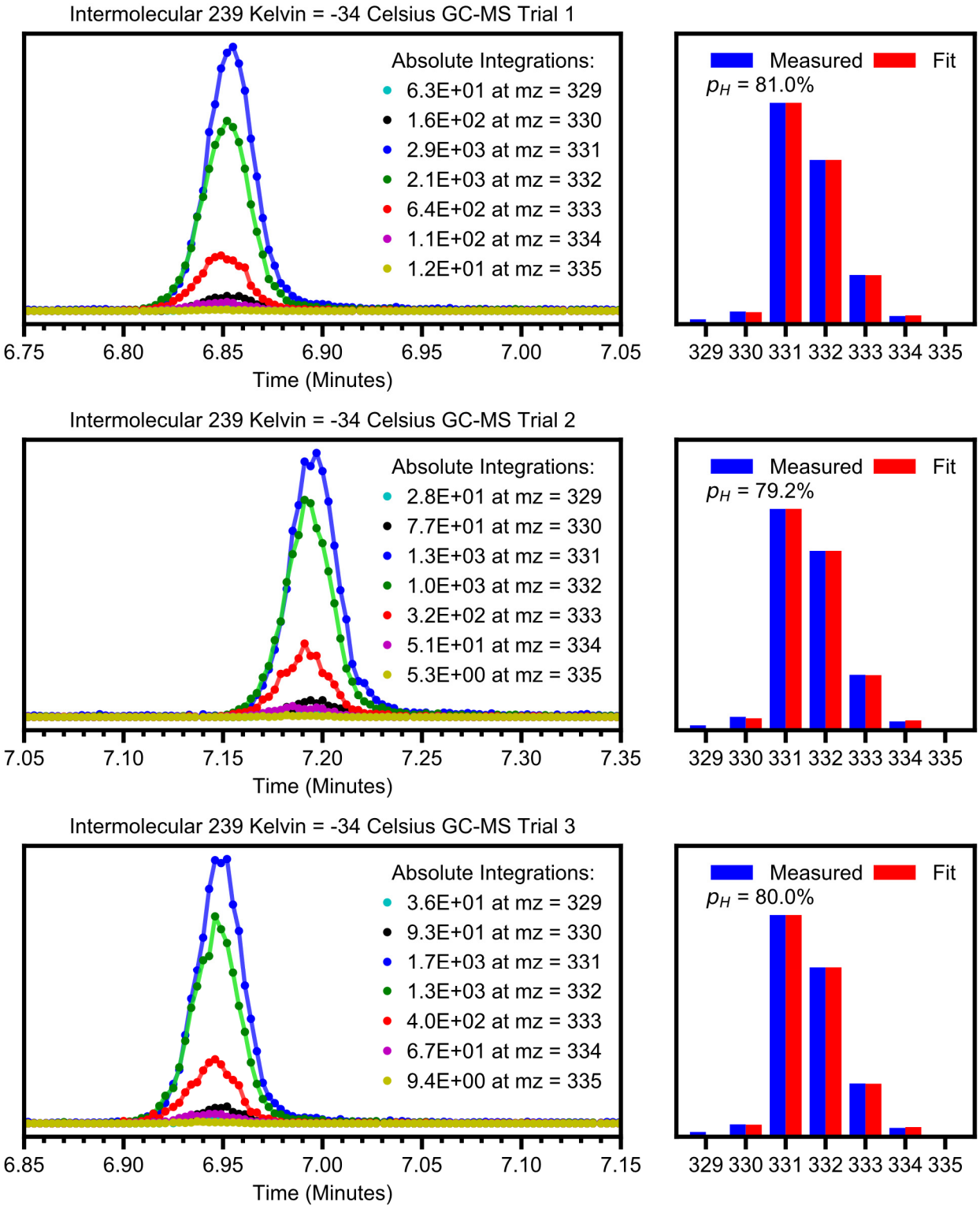

Figure S23. GC-MS data for the product analysis of the reaction of **CoO** and d_0/d_2-fluorene at 239 K.

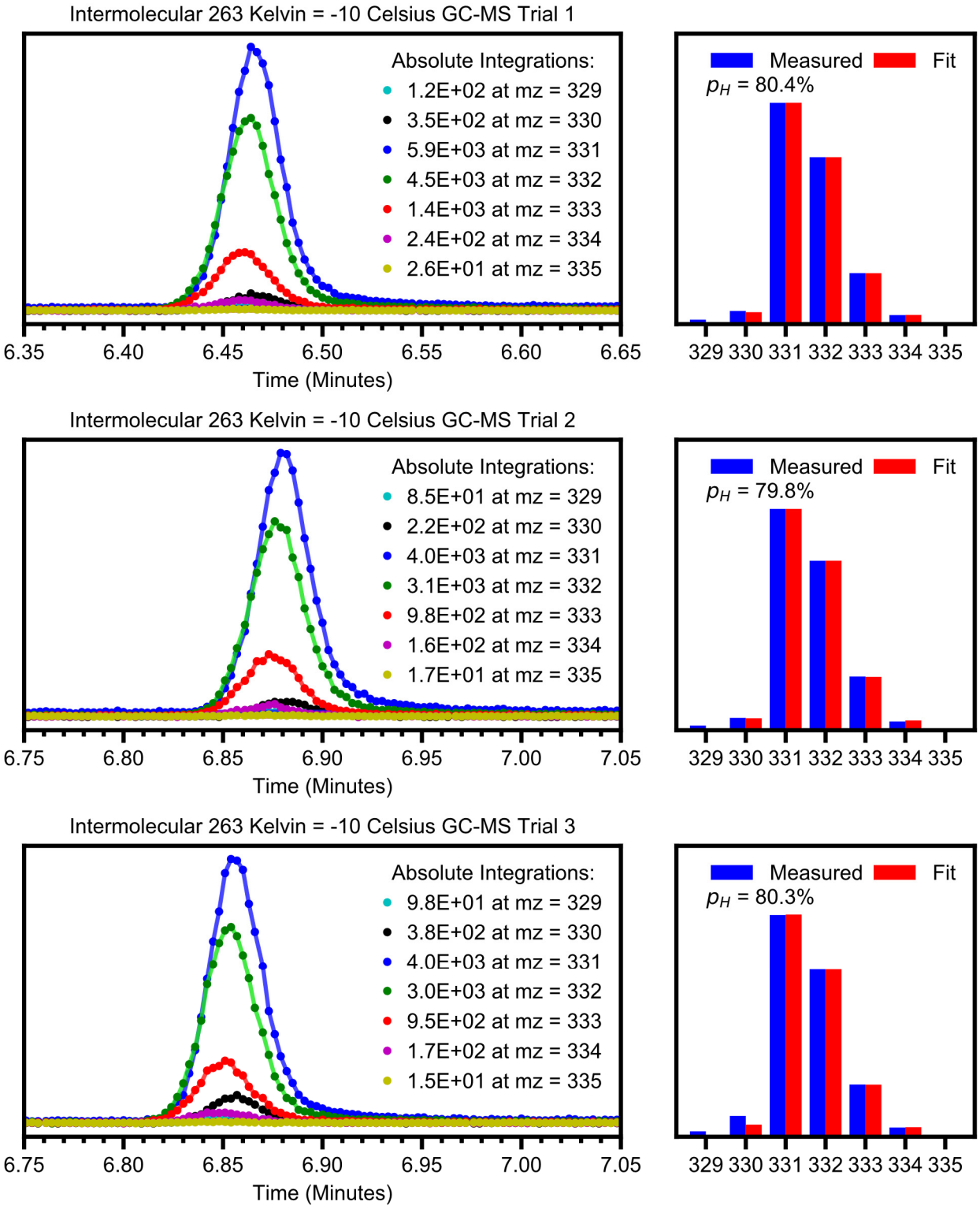

Figure S24. GC-MS data for the product analysis of the reaction of **CoO** and d_0/d_2-fluorene at 263 K.

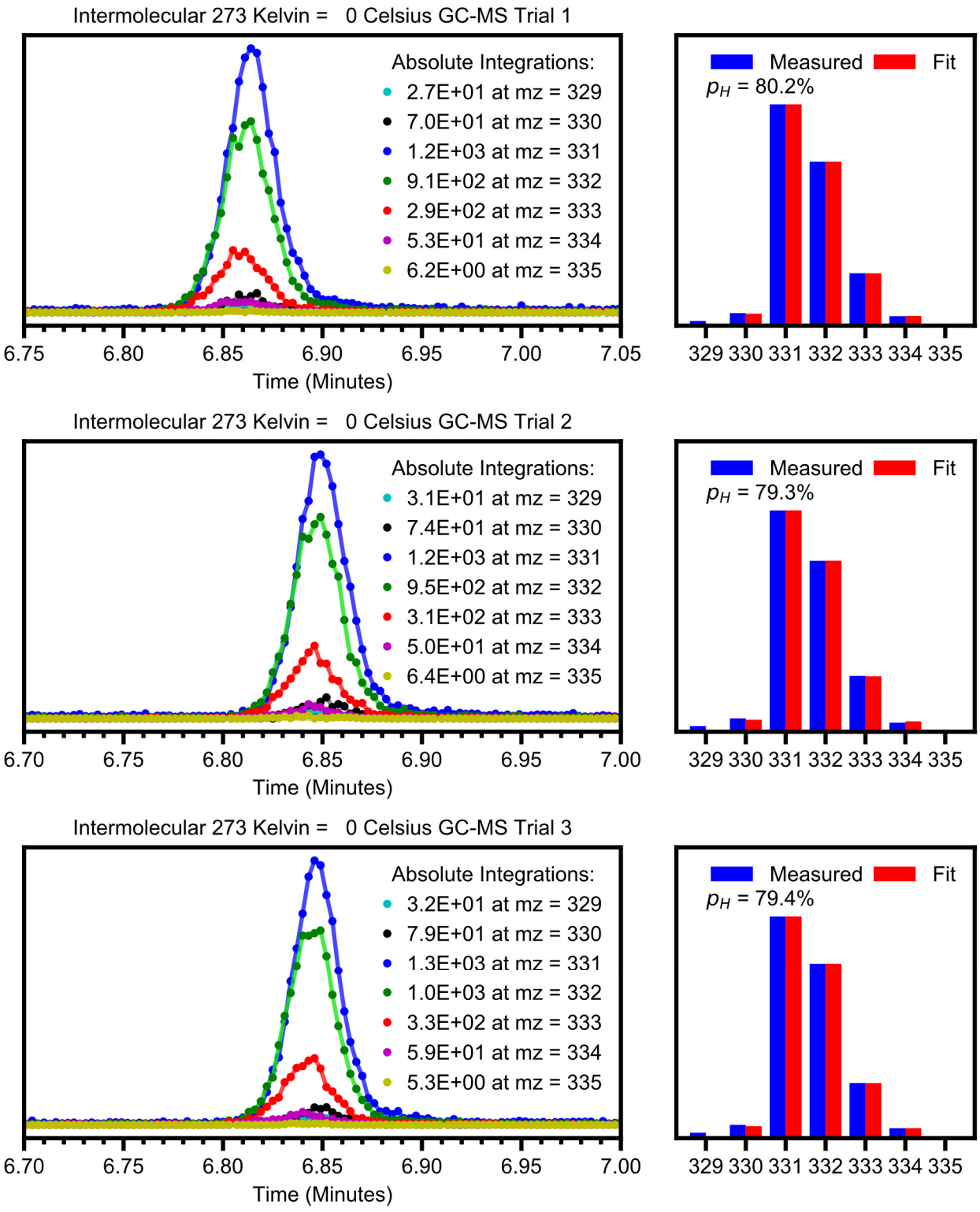

Figure S25. GC-MS data for the product analysis of the reaction of **CoO** and d_0/d_2-fluorene at 273 K.

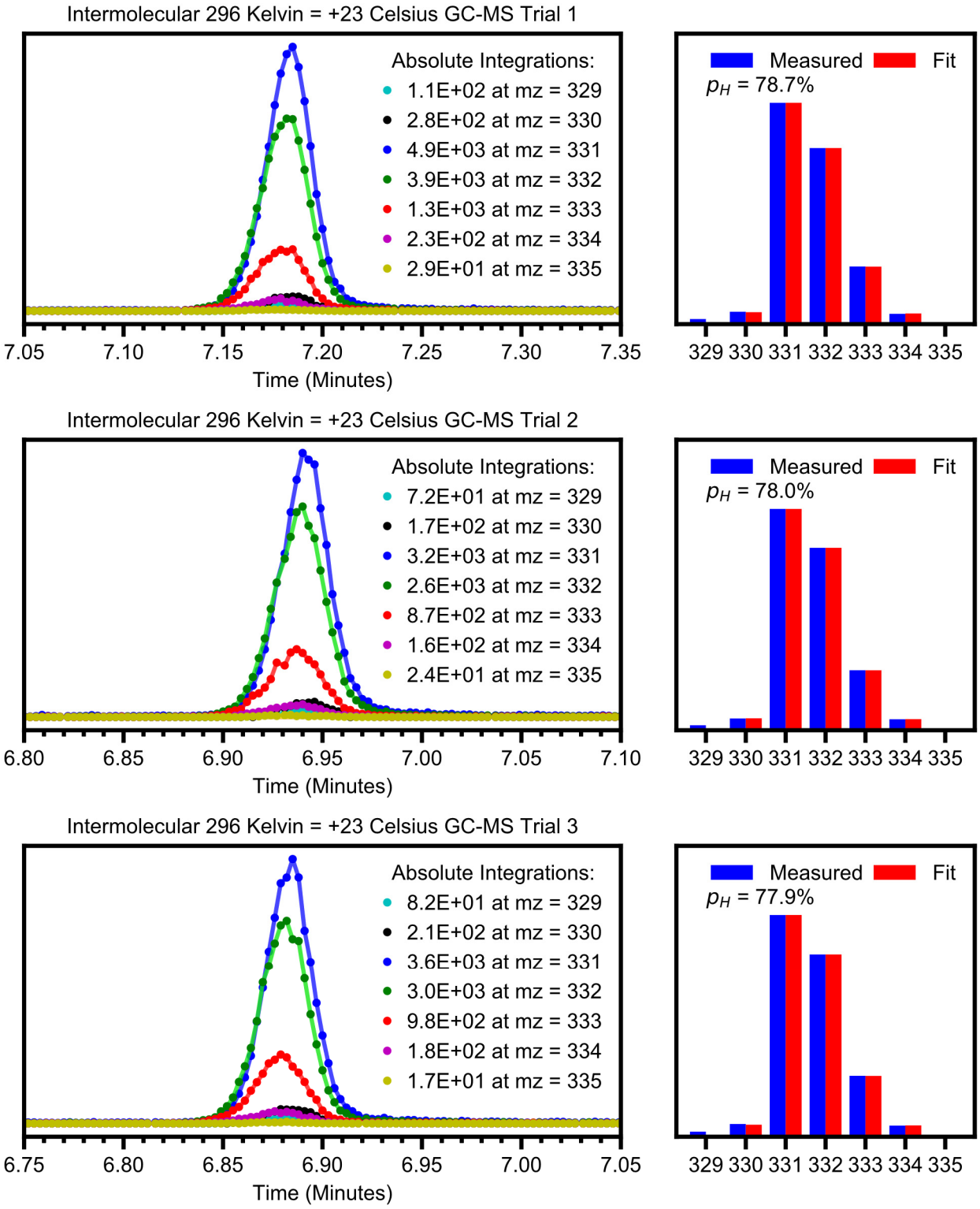

Figure S26. GC-MS data for the product analysis of the reaction of **CoO** and d_0/d_2-fluorene at 296 K.

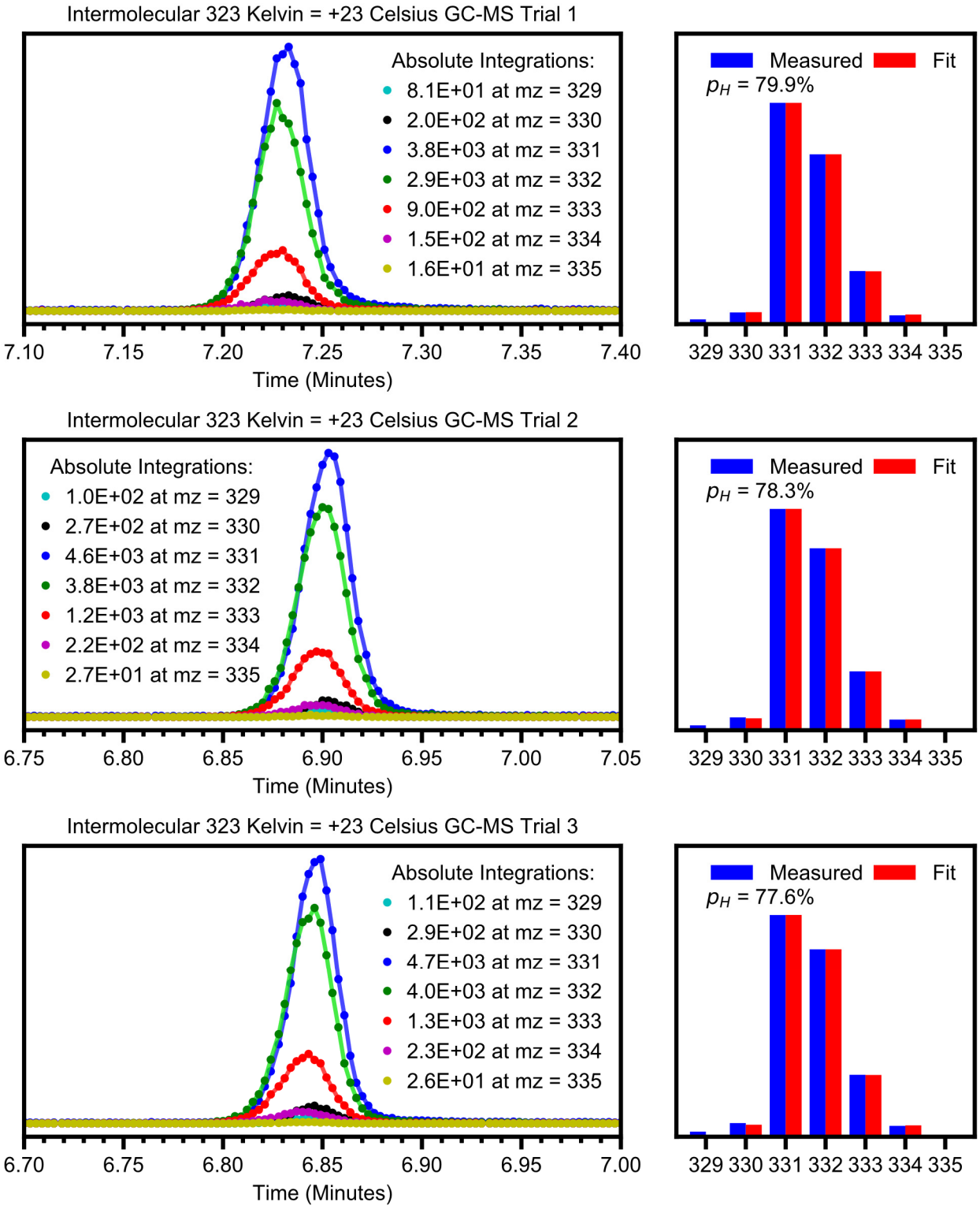

Figure S27. GC-MS data for the product analysis of the reaction of **CoO** and d_0/d_2-fluorene at 323 K.

UV-Vis Data for Kinetic Experiments

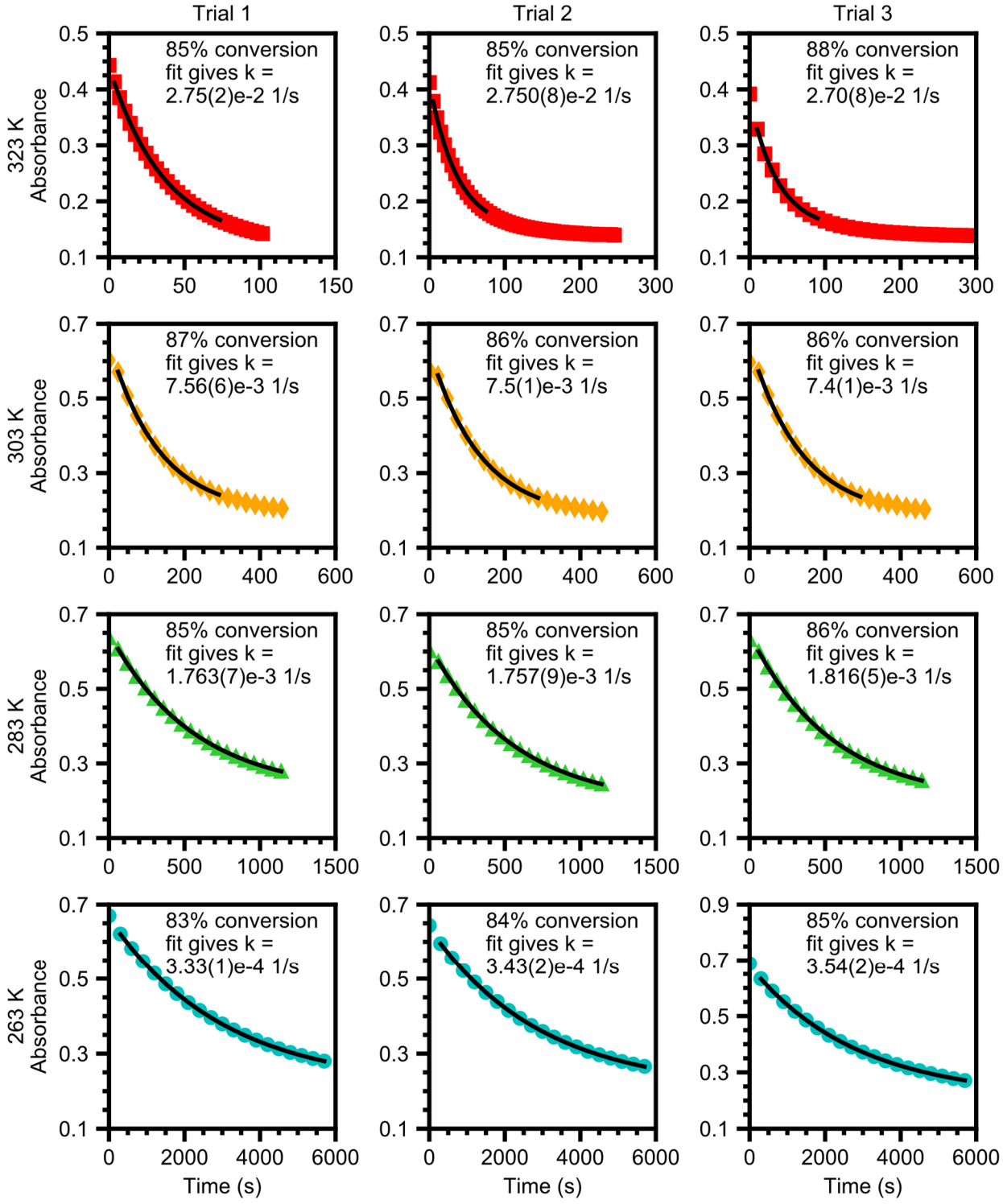

Figure S28. Plots of A vs. *t* for the reaction of **CoO** with d_0-Fluorene at various temperatures.

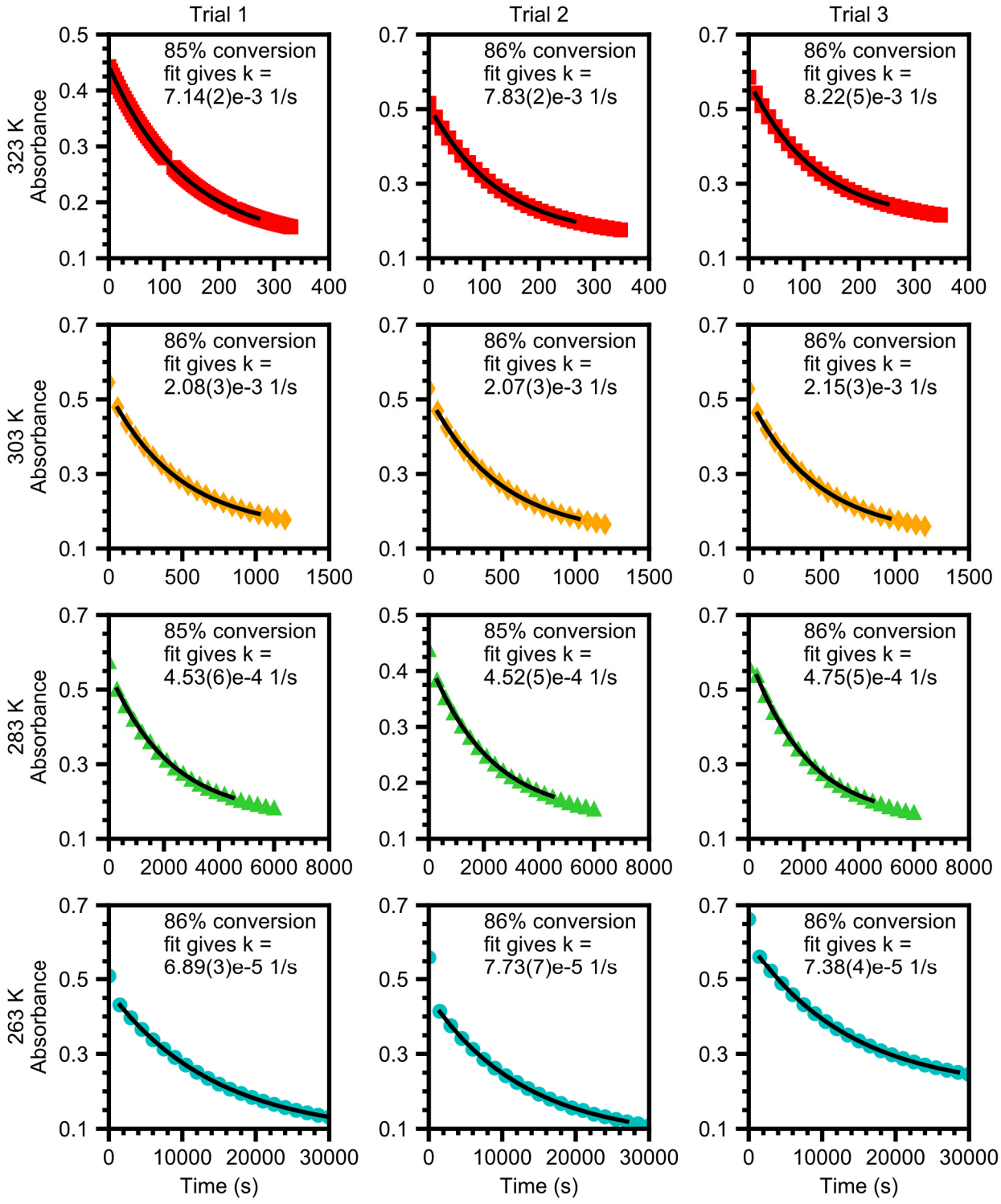

Figure S29. Plots of A vs. *t* for the reaction of **CoO** with d_2-Fluorene at various temperatures.

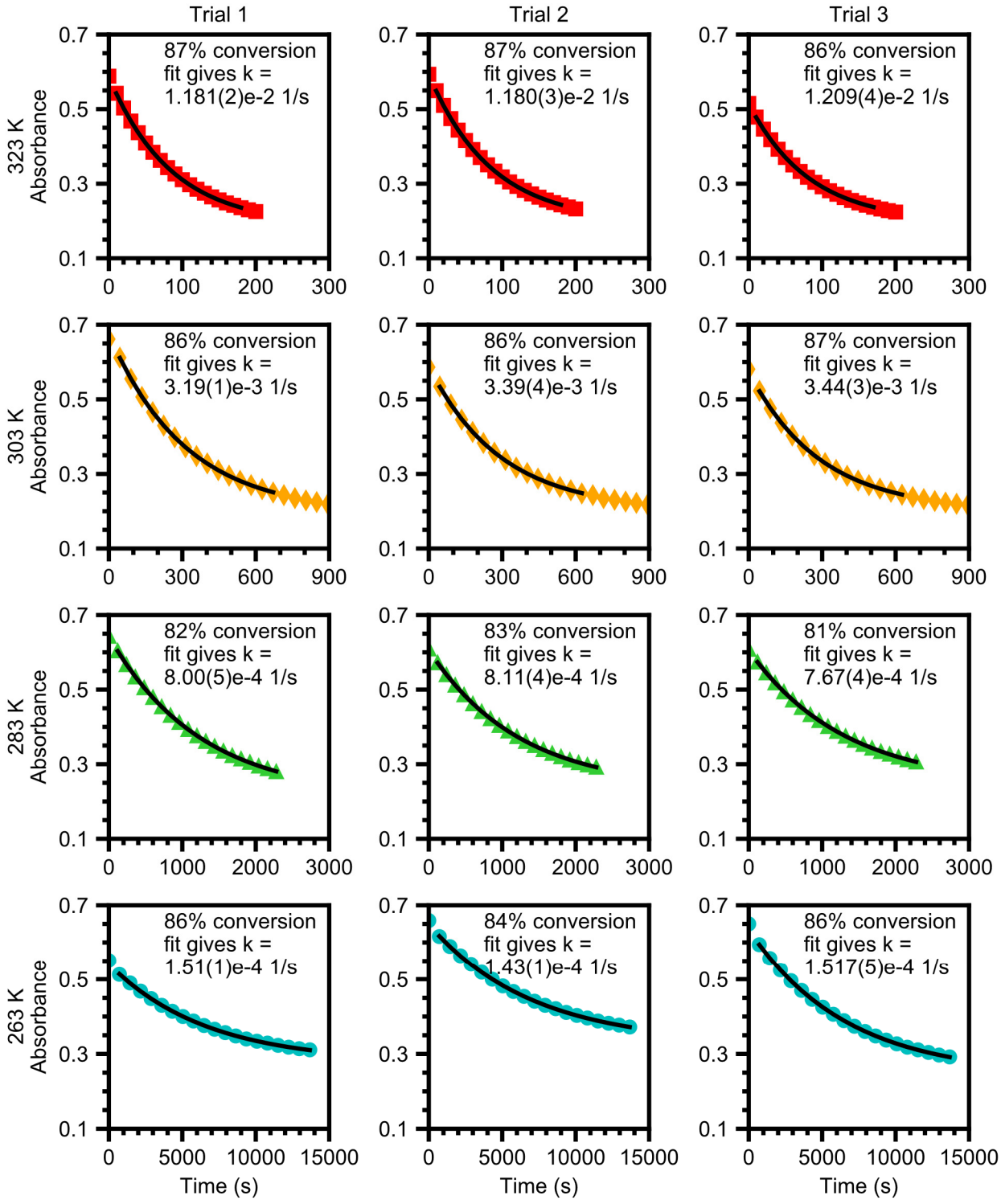

Figure S30. Plots of A vs. *t* for the reaction of **CoO** with d_0-DHA at various temperatures.

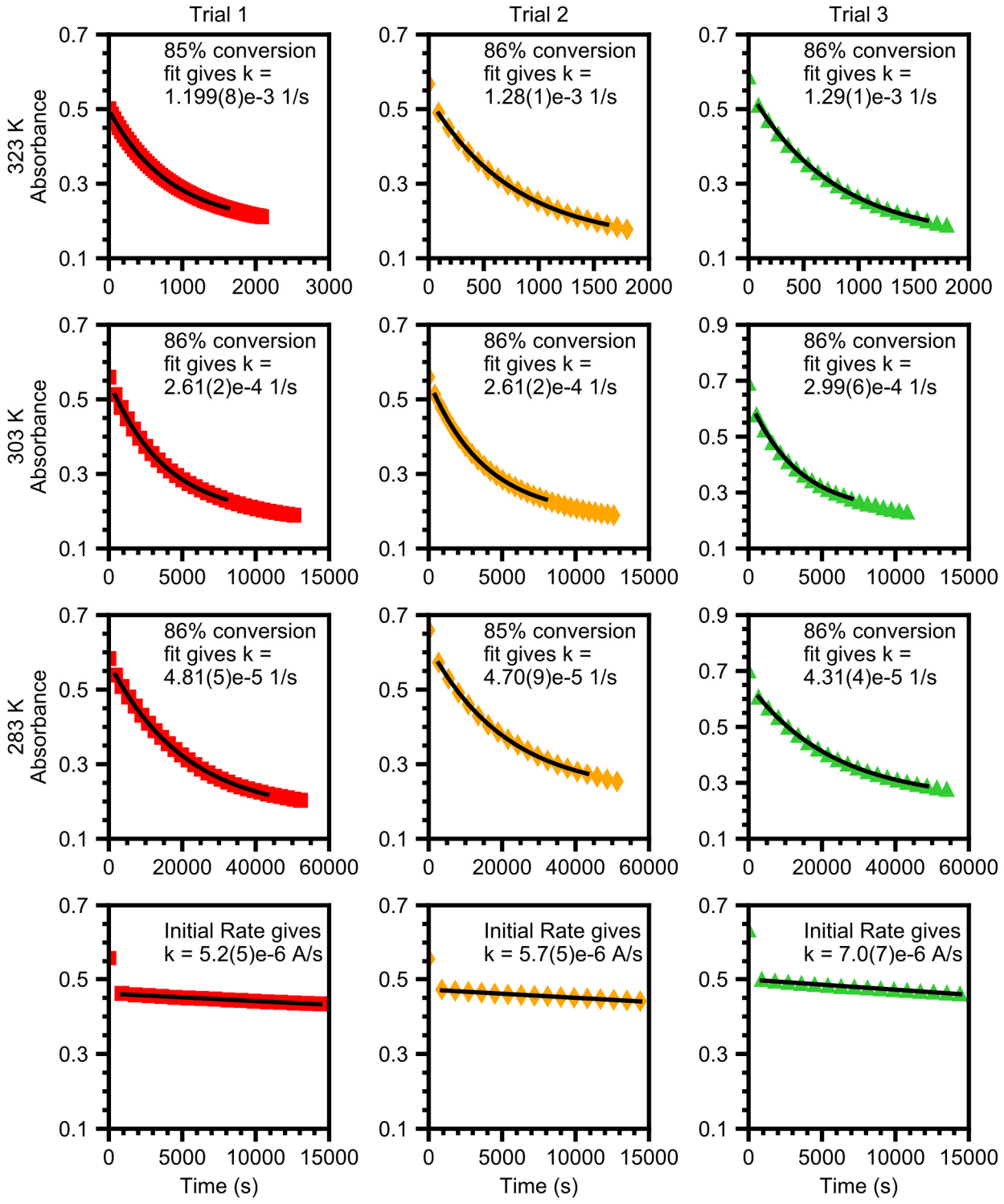

Figure S31. Plots of A vs. *t* for the reaction of **CoO** with d_4-DHA at various temperatures.

Replication of Main Text VT-KIE Figure with Expanded x-Axis

Figure S32 plot the same data as Figures 2 and 3 in the main text, respectively, but with x-axes that extend to 0 in 1/RT space.

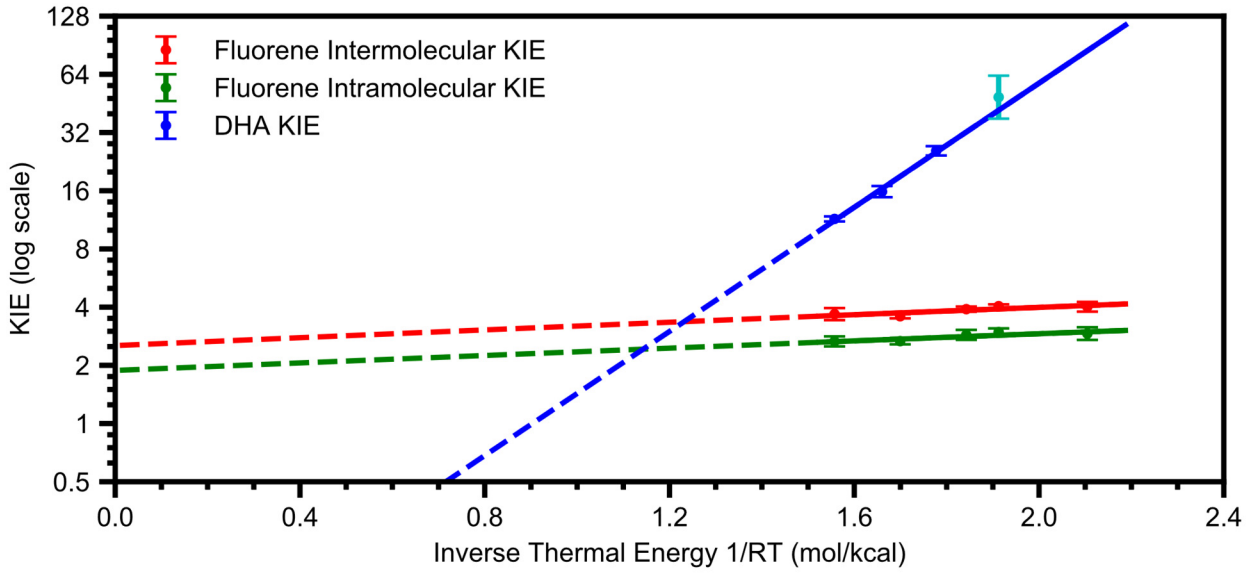

Figure S32. Plots of ln(KIE) vs 1/RT for the reactions of **CoO** with fluorene and DHA and the corresponding linear fits. The cyan colored data point at 263 K for DHA was determined via initial rates. This data point is graphed to demonstrate consistency with the other data points, but not included in the linear fits to variable temperature. The y-axis is logarithmic scale. For graphical purposes, the competition data's observed and predicted proton proportions p_H and deuteron proportions p_D are displayed as KIE $\approx p_H / p_D$ for intermolecular competition between 1:1 d_0-Fluorene d_2-Fluorene and as KIE $\approx p_D / p_H$ for intramolecular competition within d_1-Fluorene.

References

1 M. K. Goetz, E. A. Hill, A. S. Filatov and J. S. Anderson, *J. Am. Chem. Soc.*, 2018, **140**, 13176–13180.
2 C. R. Goldsmith, R. T. Jonas and T. D. P. Stack, *J. Am. Chem. Soc.*, 2002, **124**, 83–96.
3 R. J. Bailey, P. Card and H. Shechter, *J. Am. Chem. Soc.*, 1983, **105**, 6096–6103.
4 Ch. Brevard, J. P. Kintzinger and J. M. Lehn, *Tetrahedron*, 1972, **28**, 2429–2445.
5 R. P. Bell, *The tunnel effect in chemistry*, Chapman and Hall, London; New York, 1980.
6 A. Kohen and J. P. Klinman, *Acc. Chem. Res.*, 1998, **31**, 397–404.
7 J. J. Warren and J. M. Mayer, *Proc. Natl. Acad. Sci. U.S.A.*, 2010, **107**, 5282–5287.
8 I. W. C. E. Arends, P. Mulder, K. B. Clark and D. D. M. Wayner, *J. Phys. Chem.*, 1995, **99**, 8182–8189.
9 H. S. Johnston and J. Heicklen, *J. Phys. Chem.*, 1962, **66**, 532–533.
10 D. Mandal, R. Ramanan, D. Usharani, D. Janardanan, B. Wang and S. Shaik, *J. Am. Chem. Soc.*, 2015, **137**, 722–733.
11 D. Mandal and S. Shaik, *J. Am. Chem. Soc.*, 2016, **138**, 2094–2097.
12 M. Maldonado-Domínguez, D. Bím, R. Fučík, R. Čurík and M. Srnec, *Phys. Chem. Chem. Phys.*, 2019, **21**, 24912–24918.
13 M. J. Stern and R. E. Weston, *J. Chem. Phys.*, 1974, **60**, 2808–2814.